FINAL REPORT

Sediment Delivery, Trapping, and Storage during Extreme Flow Events

Hudson River Foundation Grant No. 004/13A

David K. Ralston and W. Rockwell Geyer

Woods Hole Oceanographic Institution
Woods Hole, MA 02543

January 31, 2017

ABSTRACT

Observations and a numerical model are used to characterize sediment transport in the tidal Hudson River. Study periods span a range of discharge conditions including extreme events, a typical spring freshet, and a freshet with lower than average discharge. A sediment budget for the tidal Hudson over the period 2004-2015 calculates watershed supply of approximately 12.4 MT and seaward fluxes past Poughkeepsie of 7.6 MT, representing trapping in the tidal fresh region of about 40% of the input. Sediment input from the watershed scales approximately as cubic function of river discharge, whereas seaward sediment fluxes in tidal river scale approximately linearly. Correspondingly, the tidal river accumulates sediment during the highest discharge conditions and exports during more moderate discharge. In observations, the sediment pulses associated with discharge events dissipate as they move seaward and lag the advection speed of the mean river velocity by a factor of 1.5 to 3. Idealized model cases with constant discharge ranging from 150 $m^3 s^{-1}$ to 5000 $m^3 s^{-1}$ and settling velocity from 0.01 mm s^{-1} to 3 mm s^{-1} were used to evaluate the controls on both the trapping efficiency and transport rate in the tidal river. To quantify time scales of sediment transport, the model was adapted to calculate the age of the sediment input from the watershed. The seaward transport speed of suspended sediment scaled linearly with the river velocity, but it was reduced by a lag factor that was linearly dependent on settling velocity. The lag factor was estimated to be 30-40 times the settling velocity (in mm s^{-1}), such that transport speeds that varied by several orders of magnitude from clay (~0.01 mm s^{-1}) to coarse silt (~1 mm s^{-1}). The loss of sediment due to deposition along the tidal river also depended strongly on settling velocity, and a simple advection-reaction equation could account for the loss due to settling. The time scales of sediment transport in the tidal river are slow compared to the variability in river discharge, so we used the observed discharge record and the settling velocity lag factors to statistically represent a distribution of sediment transport times through the tidal river and the estuary. The resulting time scales were long, with transport through the tidal river (to Poughkeepsie) ranging from several months to several years for settling velocities of 0.1 mm s^{-1} and 1 mm s^{-1} respectively, and transport to the Battery ranging from several years to several decades.

Preface

Please note that much of the text of this report is part of a manuscript in preparation by Ralston and Geyer for the *Journal of Geophysical Research*, as detailed in Appendix 1.

1. INTRODUCTION

Rivers provide the primary conduit for sediment delivery from continents to the coastal ocean, yet the total sediment flux that enters the coastal ocean remains difficult to constrain. Only a small fraction of global rivers have observational data on sediment delivery to the coastal zone, and in many cases those records are of only limited duration [*Syvitski*, 2003]. In rivers that are monitored, the discharge gauges are typically located above the limit of tidal influence, and thus represent the sediment delivery to a coastal region that can include extensive floodplains, tidal river, estuary, delta, and tidal flats rather than the sediment delivery directly to the ocean. Many rivers have tidal fresh regions that can extend hundreds of km from the coast and are thought to be significant sinks for sediment [*Milliman and Farnsworth*, 2013]. Estimates from major rivers indicate that up to 1/3 of the sediment delivery remains trapped landward of the coast, including the Amazon [*Nittrouer et al.*, 1995; *Dunne et al.*, 1998], Mekong [*Nowacki et al.*, 2015], Changjiang [*Milliman et al.*, 1985], and Ganges-Brahmaputra [*Goodbred Jr. and Kuehl*, 1998].

Sediment delivery from rivers is extremely episodic with discharge events, so long period of monitoring are required to capture infrequent large events to adequately characterize the sediment load. Sediment discharge (Q_s) is often related to volumetric discharge (Q_r) by a power law relationship of the form $Q_s = a\, Q_r^b$ [*Nash*, 1994]. For high discharge conditions, the exponent (b) is typically in the range of 2-3, as sediment concentration increases nonlinearly with river flow due to introduction of additional sources of sediment such as bank failure. Because of the nonlinear response, a single discharge event can deliver more sediment in a few days than several years of sediment delivery under more moderate discharge conditions. For example in Chesapeake Bay, two discharge events were estimated to have supplied half of the total sediment over a 70 year period [*Schubel and Hirschberg*, 1978]. Another study of Cheseapeake Bay found that that the fate of sediment delivered during discharge events depended in part on the settling velocity of the particles, as finer particles delivered during the

winter bypassed the estuarine turbidity maximum (ETM) while coarser sediment delivered by a smaller event in the fall were trapped in the ETM [*Sanford et al.*, 2001].

While many studies have documented sediment transport and trapping in estuaries, relatively few have investigated the transport and fate of sediment in the tidal fresh river landward of the saline estuary. The tidal river is the region that is landward of the salinity intrusion but is influenced by tides and other water level fluctuations from the coastal ocean. The landward limit of the tidal river can be a physical barrier such as a natural fall line or constructed dam, or the tidal influence can decay over a distance inland that varies depending on river discharge [*Hoitink and Jay*, 2016]. Several studies have found significant sediment trapping in tidal rivers, either by differencing upstream and downstream fluxes or by measuring accretion rates. Seaward sediment fluxes in the upper Delaware estuary exceeded the inputs from the rivers over an 8 month period of moderate-to-low discharge, suggesting an internal source of sediment stored in the tidal river [*Sommerfield and Wong*, 2011]. Sediment budget calculations for a tributary of San Francisco Bay found that nearly 50% of the sediment input was trapped in the tidal reach, and that the trapping efficiency varied on the event time scale from greater than 90% to an export 30% greater than the input [*Downing-Kunz and Schoellhamer*, 2015]. In two tributaries of Chesapeake Bay accretion rates were found to be greatest in the upper tidal fresh river and in oligohaline wetlands near the ETM, with lower accretion rates in the middle of the tidal river due to limited supply [*Ensign et al.*, 2014].

To quantify the delivery of sediment to the coastal ocean requires accounting for intermittent discharge events and sediment trapping in the tidal fresh region, and the Hudson River, which is the focus of this study, provides an example. In 2011, Tropical Storms Irene and Lee produced two major discharge and sediment delivery events within a two week period [*Ralston et al.*, 2013]. Sediment input from the storms was 2.7 MT based on measurements from gauges covering most of the watershed, about 4-5 times the long-term annual average input. Observations in the tidal river near the limit of salinity intrusion for low discharge periods found that the seaward sediment flux was only about 1.0 MT, indicating significant sediment trapping in the tidal fresh region. Other studies of high discharge conditions during the spring freshet also noted that the discrepancies between the sediment input from the watershed and the fluxes in the

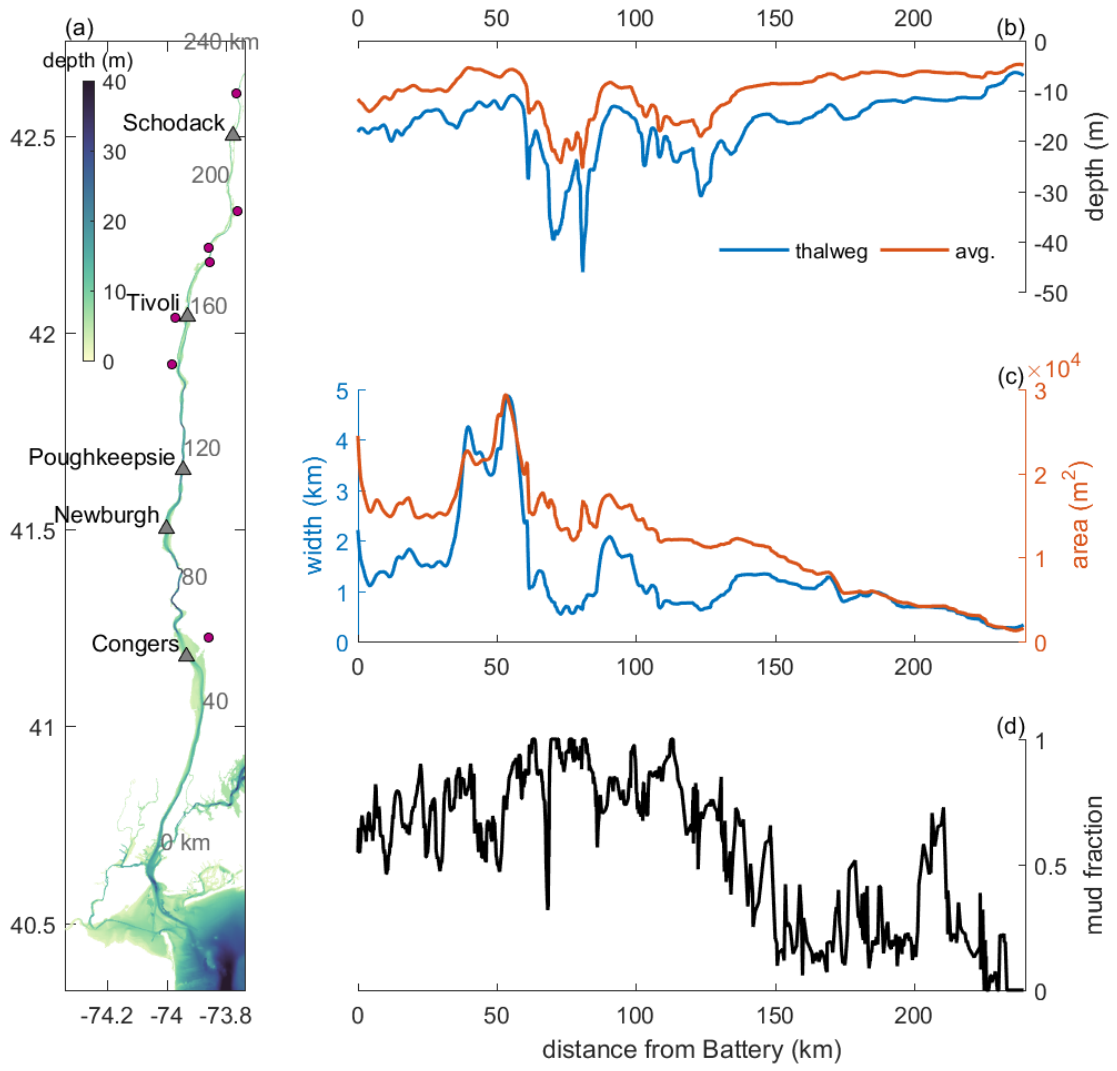

Figure 1. Hudson River bathymetry. (a) Model domain showing water depth. Observation locations are marked with triangles and locations of tributaries discharging to the tidal Hudson are marked with circles. Distance along the river from the Battery is noted in km. (b) Depth of the thalweg and cross-section average along the river. (c) Width and cross-sectional area along the river. (d) Fraction of the bed that is mud, based on the finest sediment size class in the model.

tidal river or estuary indicated extensive trapping [*Woodruff et al.*, 2001; *Wall et al.*, 2008]. These observations lead to some basic questions about the efficiency of sediment transport in the tidal river, including sediment trapping rates and transport time scales. Transport processes in the tidal river have important implications for the delivery of sediment to the coastal ocean, for transformations of sediment and organic particles between the watershed and the ocean, and for the time scales of recovery of the rivers and estuaries from particle-associated contaminants.

Here we use observations and a previously developed sediment transport model to evaluate the controls on the time scales of sediment transport in the tidal Hudson River.

2. STUDY REGION: THE TIDAL HUDSON RIVER

The Hudson River discharges into New York Harbor near the Battery at the southern tip of Manhattan, and tidal influence extends landward 240 km from the Battery to the Federal Dam in Troy, NY (Fig. 1). Mean tidal range is 1.4 m at the Battery, decreases to 1.1 m in the middle of the tidal river, and increases to 1.5 m near the head of tide. The salinity intrusion in the Hudson typically varies between 40 km from the Battery (near Piermont, NY) during high discharge conditions to 120 km (near Poughkeepsie, NY) during extreme low discharge periods [*Abood*, 1974; *Bowen and Geyer*, 2003; *Ralston et al.*, 2008]. For consistency, we define the tidal fresh Hudson as the region landward of Poughkeepsie, recognizing that during moderate and high discharge periods the fresh region extends significantly farther seaward. Channel depth decreases with distance along the river (Fig. 1), from ~17 m in the saline estuary and lower fresh tidal river (with deeper regions to 40 m) to ~10 m near the tidal limit, set by dredging for navigation to an authorized depth to Albany of 32 feet (MLW). Cross-sectional area also decreases with distance landward, from an average width of ~1.5 km near the mouth to ~0.3 km near the head of tide. Notable wider regions include the Tappan Zee and Haverstraw Bay (35-60 km) and Newburgh Bay (85-95 km).

The Mohawk and Upper Hudson rivers converge a few km above the head of tide and provide the primary source of freshwater and sediment to the tidal Hudson. The combined mean annual discharge from the Mohawk and Upper Hudson is about 400 $m^3 s^{-1}$. The Mohawk represents about 30% of the total watershed area of the tidal Hudson above Poughkeepsie, and the Upper Hudson is about 40%. Seasonally, discharge at the head of tide ranges between ~2000 $m^3 s^{-1}$ during the spring freshet to ~100 $m^3 s^{-1}$ during late summer, and large storm events can be greater than 4000 $m^3 s^{-1}$. A spring freshet of 2000 $m^3 s^{-1}$ corresponds with a mean velocity of 0.5-1.2 m s^{-1} in the upper tidal river (> 200 km), decreasing to about 0.2 m s^{-1} in the wider and deeper lower tidal river. Correspondingly, for low discharge conditions the mean velocities associated with the freshwater outflow are 0.03-0.05 m s^{-1} in the upper tidal river and less the 0.01 m s^{-1} in the lower. The tidal velocities are significantly greater than mean velocities during low and moderate discharge conditions in most of the tidal river, typically around 0.6-0.8 m s^{-1},

but during high discharge conditions the tide can become damped by the river flow and can become unidirectionally seaward in the upper tidal river [*Godin*, 1999].

Sediment discharge from the Mohawk averages 0.3-0.5 MT yr^{-1} and from the Upper Hudson 0.1-0.2 MT yr^{-1} based on records from USGS monitoring stations at Cohoes (#01357500) and Waterford (#01335770). Previous estimates range from 0.4 to 1.0 MT yr^{-1} of sediment input, reflecting interannual variability in the forcing conditions [*Panuzio*, 1965; *Bokuniewicz and Ellsworth*, 1986; *Wall et al.*, 2008]. In addition to the Mohawk and Upper Hudson, many smaller tributaries discharge directly into the tidal Hudson (Fig. 1). Collectively, these lower Hudson watersheds represent about 30% of the total area above Poughkeepsie (120 km). (The watershed downstream of Poughkeepsie is small, representing just 5% of the total watershed above the Battery.) Based on observations at Poughkeepsie, the additional volume flux from the lower Hudson tributaries increases discharge by 30-40% above the input at the head of tide [*Wall et al.*, 2008]. Various sediment flux measurements have calculated the annual sediment discharge at Poughkeepsie between 0.7 and 1.0 MT [*Panuzio*, 1965; *Bokuniewicz and Ellsworth*, 1986; *Wall et al.*, 2008]. As in most watersheds, the sediment input to the Hudson is highly episodic with river discharge. During a 4 year period of observations, an estimated 36% of the total sediment input occurred during just 3 discharge events [*Wall et al.*, 2008].

Suspended sediment concentration (SSC) in the tidal river increase during high discharge conditions, for example with tidally averaged concentrations of 40-60 mg L^{-1} at Poughkeepsie during the winter compared with ~10-20 mg L^{-1} during the summer [*Wall et al.*, 2008]. SSC also varies within the tide due to local resuspension and settling. During the winter, the tidal variability of 20-40 mg L^{-1} was observed at Poughkeepsie with a greater concentration range during spring tides, compared with tidal variability of 10-20 mg L^{-1} during summer low flow. The observations suggest that the washload of fine sediment that settles too slowly to be significantly removed from the water column during slack tide represents about half of the suspended sediment during high discharge and less than a quarter of the total during low discharge. Water samples from this location show that the suspended sediment is dominated by fines, with 90-95% of particles < 63 μm diameter; the fine fraction decreased to 80% during a high discharge event [*Wall et al.*, 2008]. This size range includes silts and clays, with particle settling velocities ranging from 3 mm s^{-1} for coarse silt to 0.01 mm s^{-1} or less for clay. At the

upper end of this settling velocity range the sediment can settle at slack tide (using a water depth of 18 m and slack duration of 1.5 hours, based on unpublished data at Poughkeepsie from G. Wall), while at the lower end of the range sediment remains in the water column at slack as washload.

The bed sediment composition in the Hudson generally becomes coarser with distance upstream of the mouth [*Nitsche et al.*, 2007]. In the saline estuary and tidal fresh to near Poughkeepsie, the bed is predominantly mud or a mix of sand and mud, with the channel being coarser and more erosional and the shoals finer sediment and more depositional. The typical grain size of the bed increases landward of Poughkeepsie, with a greater fraction of sand but also some shallow depositional regions with finer sediment. Landward of about 200 km the river is predominantly erosional and dominated by sand and gravel size classes. Most of the tidal Hudson is thought to be at equilibrium depth and accreting at a long-term rate approximately equal to sea level rise (0.3 cm yr^{-1}) based on C-14 chronology [*McHugh et al.*, 2004; *Sommerfield*, 2006]. Shorter time scale sedimentation rates from cores using Cs-137 and Pb-210 typically show higher accumulation rates, e.g. in the tidal river accumulation rates of 0.6-2.9 cm yr^{-1} at 160 km [*Benoit et al.*, 1999] and 1.5-1.8 cm yr^{-1} at 143 km [*Chillrud et al.*, 2004]. Even greater short-term accretion rates of 10-20 cm yr^{-1} have been reported in the saline estuary [*Feng et al.*, 1998; *Traykovski et al.*, 2004], although the region of the saline estuary is also thought to be in long-term equilibrium with sea level rise [*Klingbeil and Sommerfield*, 2005].

3. METHODS

3.1 Observations

Observational data were collected from several sources, including instruments deployed for this study and from long-term monitoring stations maintained by the U.S. Geological Service (USGS) and the Hudson River Environmental Conditions Observing System (HRECOS). Study periods spanned a range of river discharge conditions, included the high discharge events associated with Tropical Storms Irene and Lee in late summer 2011 (maximum discharge at the head of tide, $Q_{r,max}$ = 4400 m^3s^{-1}), a moderate spring freshet in 2014 ($Q_{r,max}$ = 2500 m^3s^{-1}), and a smaller than average freshet in 2015 ($Q_{r,max}$ = 1300 m^3s^{-1}).

Time series of river and sediment discharge were obtained from the USGS for the Mohawk River at Cohoes (1917 to present) and the Upper Hudson River at Waterford (1887 to present). Sediment discharge measurements are available for the Mohawk for 1954-1959, 1976-1979, and 2004-2015 and for the Upper Hudson for 1976-2014. River discharge, and in some cases sediment fluxes, were also obtained for tributaries of the lower Hudson River, including Normans Kill (#01359528), Kinderhook Creek (#01361000), Catskill Creek (#01362090), and Roeliff Jansen Kill (#01362182), Esopus Creek (#01364500), Rondout Creek (#01367500), and Croton River (#01375000). Volume fluxes and suspended sediment fluxes were also obtained in the tidal river at Poughkeepsie (#01372058) for 2002-2014. Details on the observations at Poughkeepsie and analysis of data from 2002-2006 can be found in Wall et al. (2008). In addition to the USGS stations, turbidity time series were obtained from several HRECOS stations on the tidal river, including Schodack Island (214 km), Tivoli Bays South (160 km), and Norrie Point (134 km).

Observations from 2011 after Tropical Storms Irene and Lee came from USGS and HRECOS monitoring stations and have been reported previously [*Ralston et al.*, 2013]. In 2014 and 2015 additional observations were collected at three locations along the tidal river: Tivoli (160 km), Newburgh (90 km), and Congers (55 km) (Fig. 1). Each location had an acoustic Doppler current profiler (ADCP) to measure velocity profiles along with, at the surface and bottom, conductivity-temperature-depth (CTD) sensors to measure water properties and optical backscatter sensors (OBS) to measure turbidity. In 2014, a particularly cold winter and extensive ice coverage delayed the start of observations until March 31, shortly before with the first discharge event of the spring freshet. Instruments were recovered June 10, 2014 when discharge at the head of tide had decreased to less than 200 $m^3 s^1$. The second deployment was from December 8, 2014 to May 15, 2015, and had generally lower than average discharge throughout the spring 2015.

Surface and bottom water samples were collected during each deployment and processed for total suspended sediment to calibrate the OBSs. The calibration between turbidity (NTU) and SSC (mg L^{-1}) from samples during the 2014 spring freshet (March 31-April 1) resulted in a regression slope of 0.6 (SSC ≈ 0.6*NTU). Our previous observations in the saline estuary using the same methods have typically found slopes of around 1, so this lower value suggests a shift in

sediment size toward smaller particles during high flow conditions. For samples taken during the lower discharge conditions of 2015 (May 13-14), the slope from the calibration to water samples was 1.1. The suspended sediment samples were also processed for loss-on-ignition (LOI), a measure of the organic content of the suspended material. For the high discharge samples of 2014 the organic content was less than 1%, while for the lower discharge samples of 2015 the LOI was 8-12%. The shift in both the turbidity-to-SSC calibration and the LOI are consistent with a greater prevalence of silt and clay particles from the watershed after the first major discharge event of the season in 2014, in contrast to 2015 when the turbidity signal was lower (shown below) and dominated by resuspended bed material with larger particles and greater organic content.

The detailed analysis presented here focuses on a subset of the observations from 2014 and 2015, but additional details and examples can be found in Appendix 2. Additional details on the observations from 2011 can be found in *Ralston et al.* [2013].

3.2 Circulation and sediment transport model

Simulations of the tidal Hudson River and estuary using realistic and idealized forcing were run using the Regional Ocean Modeling System (ROMS) with the Community Sediment Transport Modeling System (CSTMS) [*Shchepetkin and McWilliams*, 2005; *Haidvogel et al.*, 2008; *Warner et al.*, 2008]. The model has been developed and evaluated against observations over a series of previous studies [*Warner et al.*, 2005, 2010, *Ralston et al.*, 2012, 2013]. The model grid goes from the landward limit of the tidal river to open boundaries in New York Bight and Western Long Island Sound (Fig. 1). The grid resolution was 100 to 500 m along-channel with decreasing resolution toward the tidal limit, and was 20-60 m laterally. The vertical discretization had 16 evenly distributed sigma layers.

For the realistic simulations, freshwater and suspended sediment were input from the Mohawk and Upper Hudson Rivers at the head of tides as well as from the seven tributaries discharging directly into the tidal Hudson (listed above). Discharges were based on USGS observations, and suspended sediment concentrations were based on USGS observations (when available) or on rating curves developed from observations [e.g, *Woodruff*, 1999]. Water level at the open boundary was forced with tidal constituents from an ADCIRC database plus a lower frequency, non-tidal component based on a low-pass filter of water level observations at Sandy

Hook, NJ (NOAA #8531680) and Kings Point, NY (NOAA #8516945). For idealized forcing cases, river and sediment discharge were applied only at the head of tide and harmonic tides with only M_2, S_2, and N_2 components were applied at the open boundaries.

Sediment in the realistic cases was represented with 5 classes: 3 on the bed at the start of the simulation and 2 associated with river inputs. On the bed, the size classes were representative of medium sand (settling velocity, w_s = 40 mm s^{-1}), fine sand (w_s = 5 mm s^{-1}), and medium silt (w_s = 0.6 mm s^{-1}). The river sediment classes were representative of fine silt (0.2 mm s^{-1}) and very fine silt or clay (0.01 mm s^{-1}). The settling velocities of the river input sediment classes were based on previous comparisons with observations in the tidal river [*Ralston et al.*, 2013]. Maps of bed sediment composition based on side-scan surveys and bottom samples [*Nitsche et al.*, 2007] were used to create an initial distribution of bed sediment in the model, and then this was run for several months with typical forcing conditions to create an initial condition that avoided transients at startup. The bed was a single layer with a uniform initial thickness of 0.2 m.

3.3 Sediment age

To characterize the time scales of sediment transport, we modified the age calculation in ROMS that was previously used to track the chronology of water parcels [*Zhang et al.*, 2009] to apply to sediment. The mass-weighted, arithmetic age of the a tracer or of sediment is calculated following the constituent-oriented age and residence-time theory (CART) [*Delhez et al.*, 1999; *Deleersnijder et al.*, 2001]. The approach introduces an age concentration tracer that corresponding with each constituent that is being evaluated. Transport of the age concentration tracer in the model is treated exactly as the corresponding tracer, but the age grows in time with each model time step. The mean age of a tracer then is a three-dimensional (in each model grid cell), time-dependent quantity equal to the age concentration divided by the concentration of the tracer.

Sediment differs from scalars such as salinity or temperature in that mass must be tracked in the bed, and fluxes calculated between the bed and water column based on erosion and deposition rates. Similarly, the age concentration tracer in the bed and associated fluxes must be calculated, and the age concentration in the bed should increase with the model time step as in the water column. As with the sediment, the fluxes of age concentration between the bed and water column for each sediment class are assumed to be proportional to the near-bed

concentration of that sediment class for deposition or mass fraction in the surface bed layer for erosion. Transport in the water column of age concentration also corresponds to the transport of suspended sediment, with a vertical setting velocity for each sediment class in addition to advection by the 3-d velocity field. A similar application of CART to sediment was used to calculate sediment age off the Belgian coast, except in that application sediment resupsended from the bed was set to have zero age, and age was not tracked in the bed [*Mercier and Delhez*, 2007]. In the Hudson simulations, sediment continues to age after deposition and resuspended sediment takes with it the age concentration of the bed. The sediment on the bed at the start of the simulation continues to age with linearly with model time, and thus is not of particular utility for further analysis. The analysis here focus on the age of sediment introduced with river discharge, which is tracked as sediment classes distinct from the initial bed sediment. Sediment from the watershed enters with zeros age concentration and ages as it moves through the system, with a spatial distribution of the age of sediment in suspension and on the bed that depends on sediment properties, in particular settling velocity.

4. RESULTS

4.1 Sediment fluxes and mass accumulation

The major discharge events associated with Tropical Storms Irene and Lee in late summer 2011 delivered about 2.7 MT of new sediment to the tidal Hudson. Due to the rainfall distribution, disproportionate sediment loading came both from the Mohawk (1.4 MT, 30% of the total watershed area) and from several tributaries discharging directly to the tidal Hudson, in particular Catskill Creek (0.7 MT, 3% of total watershed, located at 180 km) [*Ralston et al.*, 2013]. At Poughkeepsie, the cumulative flux during the months following the storms was about 1.0 MT, indicating that a substantial fraction of the total sediment input remained in the tidal river for a period much greater than the event or spring-neap time scale. Fortunately, the Irene and Lee events occurred during a period of expanded monitoring of sediment discharge by the USGS for the watersheds of the lower Hudson. Streamflow and suspended sediment concentrations were recorded at stations representing most of the total watershed area, allowing quantification of the tidal river sediment budget to an uncommon precision.

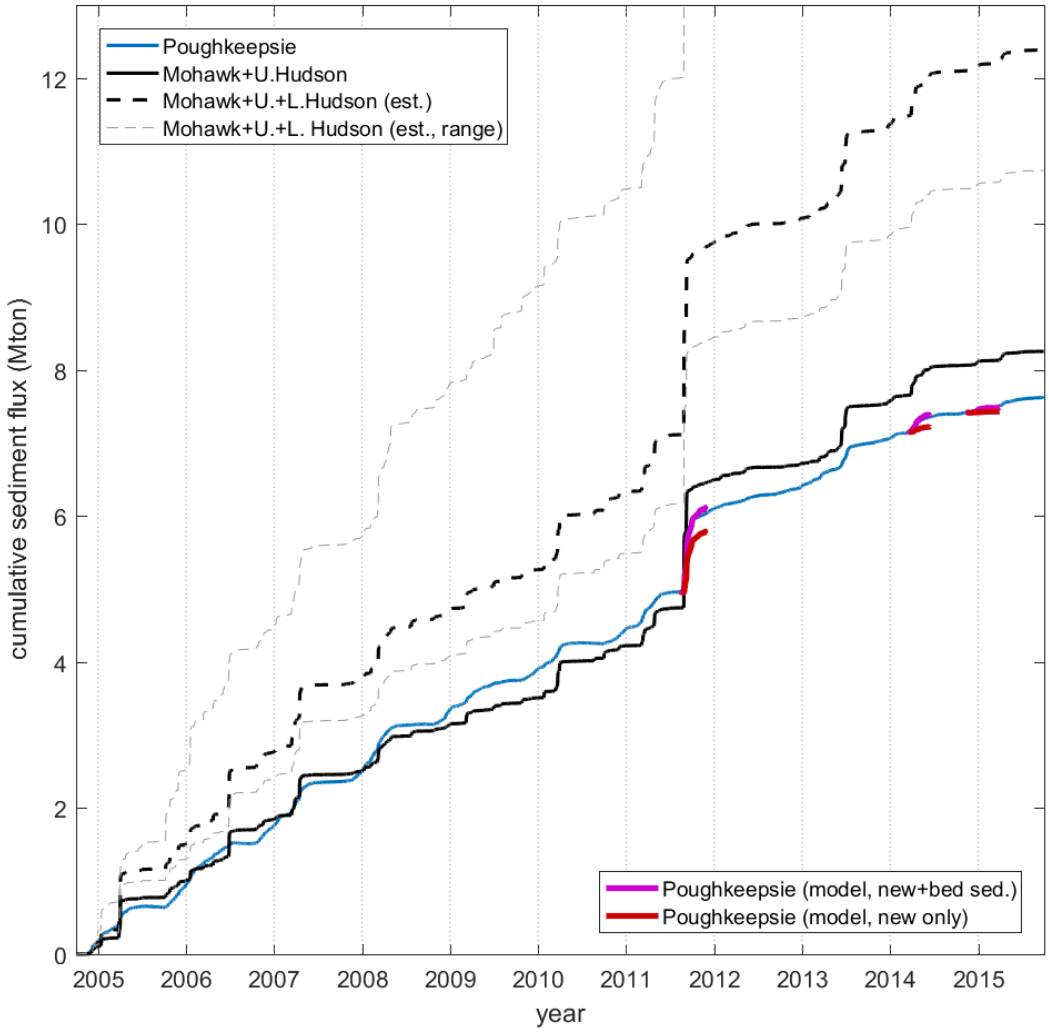

Figure 2. Cumulative sediment flux in the tidal Hudson. Observed fluxes at Poughkeepsie are based on measured velocity and suspended sediment (USGS), or when that is not available, on velocity at Poughkeepsie and suspended sediment from turbidity at Norrie Point (HRECOS). Sediment inputs measured for the Mohawk and Upper Hudson are shown along that times a factor of 1.5 to account for additional inputs from Lower Hudson tributaries, as noted in the text. Cumulative sediment flux at Poughkeepsie for each of the model periods (2011, 2014, 2015) are shown for both new sediment from the watershed and new sediment plus remobilized bed sediment.

One of the key uncertainties in the sediment budget is the loading from tributaries discharging directly to the tidal Hudson. For Irene and Lee, the Lower Hudson tributaries increased sediment loading by about 70% above that from the Mohawk and Upper Hudson. An estimate based on the difference between the Mohawk and Upper Hudson loading and the flux at Poughkeepsie over 4 years calculated that the increase in sediment loading from the Lower

Hudson was 30-40% [*Wall et al.*, 2008]. As with Irene and Lee, the largest imbalances between the input at the head of tide and the flux past Poughkeepsie were associated with high discharge events. In another study, contaminant metal profiles from sediment cores along the tidal fresh Hudson were used to calculate that Upper Hudson sediment was being diluted by a factor of 8 [*Chillrud et al.*, 2004]. The sediment load from the Mohawk on average is 2.6 times that of the Upper Hudson, so the Upper Hudson sediment dilution observed in the cores requires an additional sediment input from tributaries of the Lower Hudson that is similar in magnitude to the combined input from the Upper Hudson and Mohawk. A watershed model accounting for differences in land use suggested that sediment yield (mass per area) for the Lower Hudson was greater than for the Upper Hudson [*Swaney et al.*, 1996], consistent with an input proportionally greater than the watershed area ratio.

Daily averaged sediment discharge measurements are all available for the Mohawk, Upper Hudson, and tidal fresh Hudson at Poughkeepsie for most of the period 2004-2015 (Fig. 2). For the periods when SSC data are not available at Poughkeepsie (9/2011-1/2014 and 10/2014-10/2015), SSC data from Norrie Point are paired with the volumetric discharge at Poughkeepsie. During Irene and Lee, Norrie Point turbidity was found to correlate well with turbidity observed at the Poughkeepsie water treatment plant [*Ralston et al.*, 2013]. Turbidity at Norrie is converted to SSC based on a calibration from bottle samples. To estimate the total sediment load to the tidal river including tributaries of the Lower Hudson, the observed fluxes from the Mohawk and Upper Hudson have been multiplied by a factor of 1.5. This factor is an average of previous estimates of 1.3 [*Wall et al.*, 2008] and 1.7 [*Ralston et al.*, 2013], and is significantly less than the 2.2 factor derived from concentrations of contaminant metals in cores [*Chillrud et al.*, 2004]. Over this 11-year record, the cumulative input from the Mohawk and Upper Hudson was 8.2 MT, and with the 1.5 factor for the Lower Hudson tributaries is a total estimated input of 12.4 MT. At Poughkeepsie, the cumulative seaward flux was 7.6 MT, somewhat less than the input at the head of tides and about 60% of the total estimated sediment input from the watershed.

The trend over this 11-year period indicates that some 40% of the watershed input remains trapped in the fresh tidal river for an extended period. The spatial extent of the tidal fresh Hudson above Poughkeepsie is about 110 km^2 (120 km of river with average width of~900

m), so assuming a bulk density of 500 kg m^{-3} the calculated mass accumulation distributed evenly would correspond with a depositional thickness of 8.5 cm. Sea level rise at the Battery is 3.38 mm yr^{-1} (1975-2015, https://tidesandcurrents.noaa.gov/sltrends/50yr.htm?stnid=8518750), equal to 3.7 cm over 11 years, so the increase in accommodation space is similar in magnitude to the sediment trapping. The depositional area may be an overestimate given that large parts of the tidal fresh Hudson are sandy and non-depositional [*Nitsche et al.*, 2007], but additional sediment storage is possible on flood plains or in off-river water bodies, where accumulation rates can greatly exceed sea level rise [*Woodruff et al.*, 2013]. As noted above, cores from depositional regions along the tidal fresh Hudson have been found to have accumulation rates in excess of 1 cm yr^{-1} [*Benoit et al.*, 1999; *Chillrud et al.*, 2004].

In previous work, the cumulative sediment fluxes past Poughkeepsie after Irene and Lee were found to be similar in the model as in the observations [*Ralston et al.*, 2013]. The settling velocity associated with the river input sediment was a critical parameter that was adjusted to improve the agreement with the observations. The watershed inputs were split into sediment classes with w_s = 0.2 mm s^{-1} (17 m d^{-1}) and 0.01 mm s^{-1} (0.8 m d^{-1}), corresponding respectively with particle sizes of fine to medium silt and fine silt or clay that settles at rates much slower than the tidal time scale. We show later that the mean advection speed for sediment decreases as settling velocity increases, so the timing and quantity of mass flux past a location in the model depends on the fraction of the total sediment input assigned to the washload. For Irene and Lee, assigning 20% of the new sediment to the washload size class agreed with the mass flux observations, so that ratio is used in the realistic simulations in this study. The Irene and Lee model results also demonstrated that matching the timing of the fluxes past Poughkeepsie required including remobilization of bed sediment in the river prior to the events. The total transport in the model then depends not only on the watershed inputs, but also the availability of erodible sediment in the antecedent bed conditions.

The model was also run for the observational periods in 2014 and 2015 with the configuration used for Irene and Lee, and the net flux in the model at Poughkeepsie for those periods compares well with the observations (Fig. 2). Again, the total mass flux, including remobilized bed sediment, is closer to the observations than the river input sediment alone. 2014

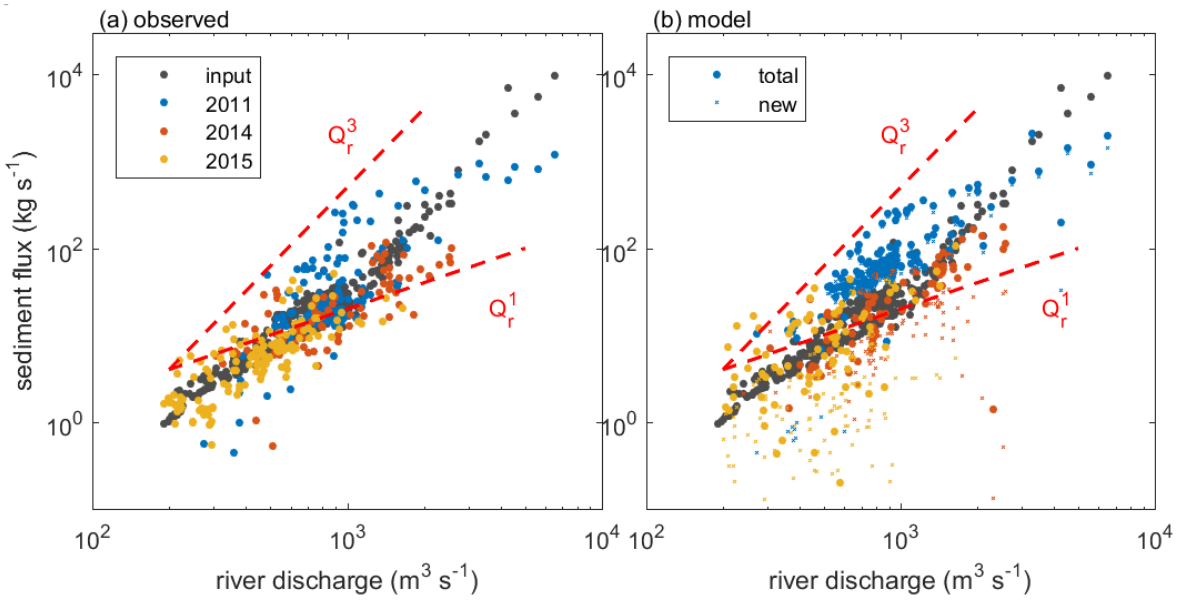

Figure 3. Sediment flux vs. river discharge. (a) Sediment input from rivers (black) and sediment flux at Poughkeepsie during 2011, 2014, and 2015 observation periods. (b) Sediment flux at Poughkeepsie in the model during the same periods; river inputs are the same. Large dots are the total sediment flux including remobilized bed sediment, and small x's are newly input sediment from the rivers.

had a typical spring freshet, and the total sediment flux past Poughkeepie during the simulation period (85 days) was 0.20 MT in the observations and 0.24 MT in the model. Estimated watershed input during that same period was 0.35 MT. In 2015, the freshet discharge was lower than average and the sediment fluxes were also reduced, with 0.087 MT observed past Poughkeepsie and 0.067 modeled over 135 day period, compared with 0.071 MT of watershed input.

Both the observations and the model reflect the strong dependence on discharge of both the watershed sediment loading and the flux in the tidal river. For the Mohawk the sediment discharge rating curve is $Q_s \sim Q_r^{1.35}$ for $Q_r < 500$ m^{3}s^{-1} and $Q_s \sim Q_r^{2.87}$ higher discharge [*Woodruff*, 1999]. In the Upper Hudson the relationships are similar, with $Q_s \sim Q_r^{1.43}$ for $Q_r <$ 400 m^{3}s^{-1} and $Q_s \sim Q_r^{2.87}$ for greater discharge. Because of the nearly cubic dependence on river discharge, the sediment loading to the tidal river is dominated by large, infrequent events. In contrast, the relationship between volumetric discharge and sediment flux at Poughkeepsie in both observations and the model is weaker than the cubic dependence of sediment supply (Fig. 3). During the peak flows of Irene and Lee, the watershed supply exceeded the observed flux in the tidal river by an order of magnitude. At intermediate discharges near the annual average, the

seaward flux at Poughkeepsie was similar to or greater than the watershed input. The interannual variability in flux at intermediate discharges depends in part on the availability of mobile sediment, which depends on the antecedent loading to the system. In 2011, the supply of mobile sediment in the tidal river was enhanced due to the inputs from the two storms, and consequently sediment concentrations were greater at given discharge than in the subsequent years. Overall, the flux at Poughkeepsie scales roughly linearly with river discharge, with the magnitude of the linear dependence varying with sediment concentration due to antecedent loading conditions. Assuming that at long time scales the system is morphdynamic equilibrium, the mismatch in scaling between the nearly cubic sediment supply and the linear transport requires that there is a net sediment gain to the tidal river during brief high discharge events and net loss over longer periods of intermediate discharge [*Ralston and Geyer*, 2009]. This pattern of sediment accumulation during events and net loss during lower discharge periods is consistent with previous analysis of a four year record at Poughkeepsie [*Wall et al.*, 2008]. The roughly linear scaling of the sediment flux in the tidal river is reproduced in the model with interannual variation similar to the observations, but only when including the seaward flux of remobilized bed sediment (Fig. 3b).

4.2 Sediment transport time scales

The discrepancy in discharge dependence between the watershed loading and the sediment flux in the tidal river raise questions not only of total sediment mass flux but also of timing. Observations of turbidity at multiple locations along the tidal fresh river can illustrate the advection of the sediment pulses associated with river discharge events (Fig. 4). In 2011, Irene and Lee ($Q_{r,max} \approx$ 3900 and 3300 m^3s^{-1} at the head of tide) each provided distinct peaks in turbidity at Schodack (214 km), Tivoli (160 km), and Norrie Point (134 km). The seaward advection of the turbidity pulse can be compared with the advection speed based on the mean river velocity, $U_r = Q_r/A$, where A is the average cross-sectional area of the river. The turbidity pulse moved seaward more slowly by a factor of 1.5 to 2 than the advection time based on the average river velocity between the stations. The calculation was based on the arrival time of the peak turbidity for each discharge event, which has uncertainty that grows as the turbidity pulse spreads during advection downstream. Similar lags of 1.5 to 2 were found based comparing the

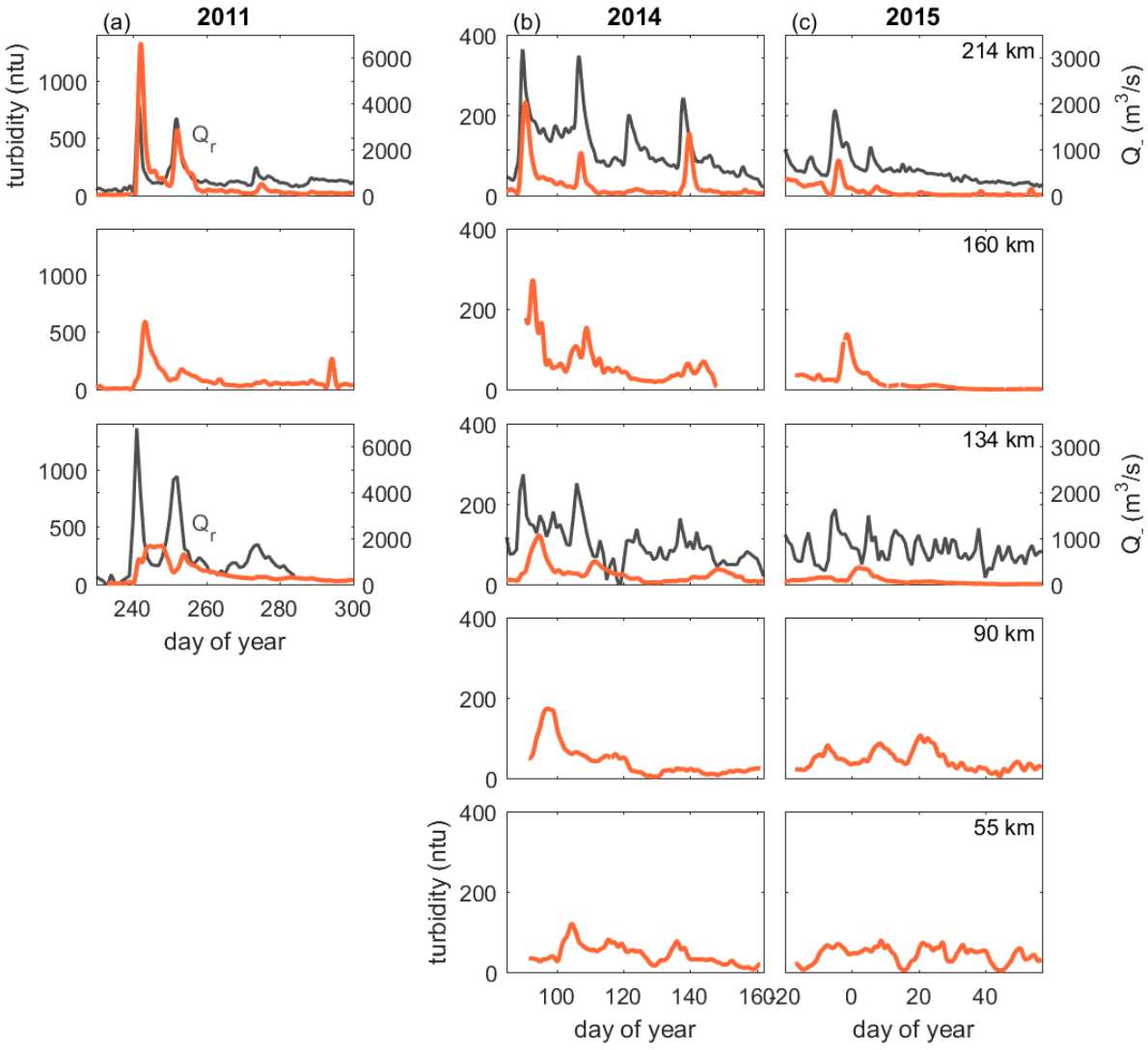

Figure 4. Observed time series of turbidity along the Hudson at Schodack (214 km), Tivoli (160 km), Norrie Point (134 km), Newburgh (90 km) and Congers (55 km) during the 2011, 2014, and 2015. Note that the turbidity axis range for column (a) is 3.5x greater than for (b) and (c). River discharge at the head of tide and mean flow at Poughkeepsie are shown in black on the right axis.

propagation speed of the observed turbidity signal with the tidally averaged velocities from the model rather than Q_r/A.

In the spring of 2014, three distinct discharge events ($Q_{r,max} \approx 3200, 3000, 2100$ m^3s^{-1}) were associated with spikes in turbidity that could be tracked through the tidal river, with additional sensors in place at Newburgh (90 km) and Congers (55 km) (Fig. 4b). The spring of 2015 had lower discharge conditions, with only a single event ($Q_{r,max} \approx 1800$ m^3s^{-1}) that had a

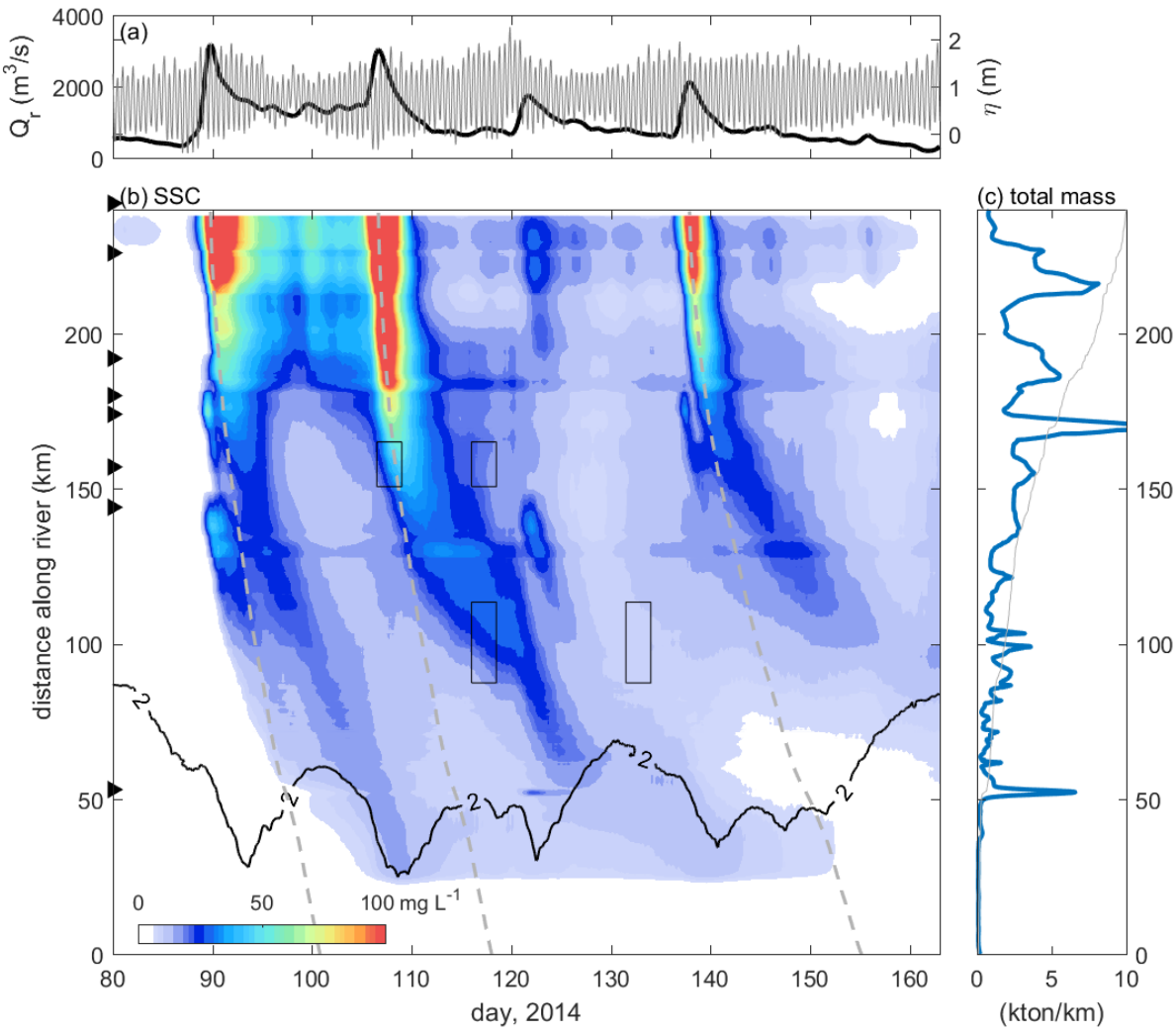

Figure 5. Modeled time series of suspended sediment from river inputs in 2014. (a) River discharge at the head of tide and water level at the Battery. (b) Cross-sectionally averaged suspended sediment concentration from river inputs as a function of distance along the river and time. Tributary inputs are marked with triangles on the y-axis. The rate of advection associated with the three largest discharge events (distance = $\Sigma(Q_r/A)\Delta t$) is marked with a gray dashed line. The 2-psu isohaline of bottom salinity is marked in black. Boxes highlight the periods and locations shown in Fig. 6. (c) Total sediment mass (suspended + bed) at the end of the model period. Gray line is the cumulative mass distribution from the seaward boundary to the head of tide normalized by the total mass.

distinct turbidity signal through the tidal river. At the more seaward observation locations the turbidity maxima from the discharge events become more diffuse and hard to identify, and instead the spring-neap cycle was most prominent in the temporal variability. While the mean flow U_r is responsible for the net seaward transport, the tidal velocities that are typically an order or of magnitude greater enhance along-river dispersion of the turbidity pulse and obscure the signal. For the larger discharge events that could be tracked, the turbidity signal again moved

seaward at a rate slower than river flow. The transport time between stations was 1.5 to 3 times the transport time for water, with the factor generally increasing between the more seaward locations. Note that the turbidity signal may represent only a portion of the sediment input associated with a discharge event, in particular the finer, slower settling particles that are transported most efficiently.

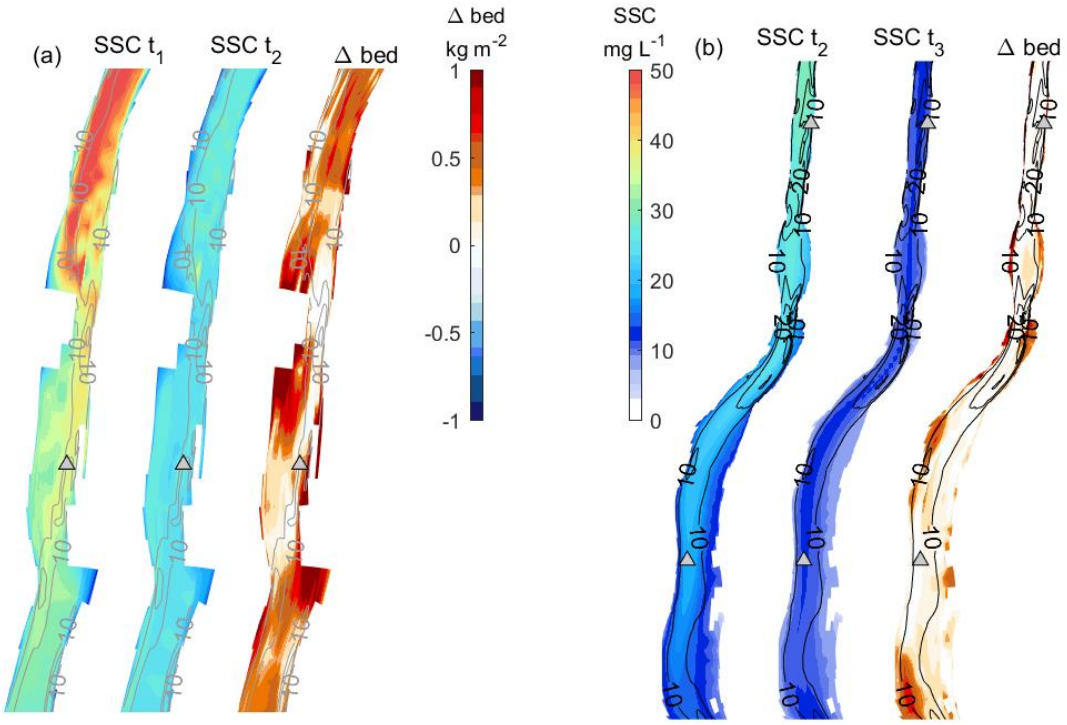

Figure 6. Maps of average suspended sediment concentration from river inputs for two times and the net change in sediment mass on the bed between the periods. Selected times are during a period with increased sediment concentration from a discharge event and then 10-15 days after. Two regions are shown, (a) near Tivoli and (b) near Poughkeepsie and Newburgh; locations of the observations are marked with gray triangles. The times and locations of the maps are marked in Fig. 5.

The model results provide more continuous picture in time and space of the suspended sediment mass distribution resulting from discharge events (Fig. 5). The spring freshet of 2014 is used as an example here, but similar results were found for 2011 [*Ralston et al.*, 2013] and for 2015. Three discharge events provided significant sediment loading, and the advective time scale based on Q_r/A for each is noted for reference. Note that this realistic simulation includes river and sediment discharge from lateral tributaries of the Lower Hudson that provide river inputs prior to the arrival of the sediment pulse from the Mohawk and Upper Hudson. The model results illustrate spatial variability that is not resolved by the observation time series, as greater

suspended sediment concentrations are consistently found in particular regions along the river. The sediment inputs from each event highlight these local trapping regions, but the seaward advection of the sediment pulse can be tracked downstream as it disperses and lags the rate of advection by the river velocity. The realistic results for 2014 (Fig. 5) combine sediment classes with 0.01 and 0.2 mm s^{-1} based on the Irene and Lee calibration, but as will be examined later with idealized model cases, the sediment transport rate relative to river advection is sensitive to the settling velocity.

As the suspended sediment pulse associated with each discharge event moves down the river, it spreads and the maximum sediment concentrations decreases. Between discharge events, suspended sediment concentrations decrease more, as the elevated river velocity during the event that helped keep sediment in suspension decreases. After each event, tidal velocities continues to remobilize and move sediment and sediment is preferentially deposited in lower energy regions on the shoals and side embayments. Examples from the model during and after the arrival of an event sediment pules demonstrate the temporal decrease in SSC corresponding with accumulation in at the channel edges (Fig. 6). Locations of the observation time series of turbidity are also marked, and the model provides context for the spatial gradients associated with the bathymetric and sedimentary structure. In these simulations the model did not allow wetting and drying, but a similar redistribution of sediment in suspension during discharge events to longer term storage on floodplains would be expected.

The along-river distribution of newly input sediment at the end of the simulation period, including both sediment in suspension and on the bed, highlights both the regions of intensified trapping and the overall retentiveness of the river (Fig 5c). Over approximately 3 months, about 0.34 MT of sediment were introduced to the system, predominantly during the discharge events 10 and 15 days into the simulation. Some of that new sediment moved down into the saline estuary, and much of it that did was trapped in the upper ETM of Haverstraw Bay (55 km) [*Nitsche et al.*, 2010; *Ralston et al.*, 2012]. However, only about 15% of the total sediment input moved seaward of the limit of the salinity intrusion, which at the end of the simulation was located at 90 km, and less than 1% moved seaward of the Battery. As with the rate of sediment transport, we will examine with idealized cases how the sediment trapping in the tidal river (or inversely, the transport efficiency) depends greatly on the settling velocity.

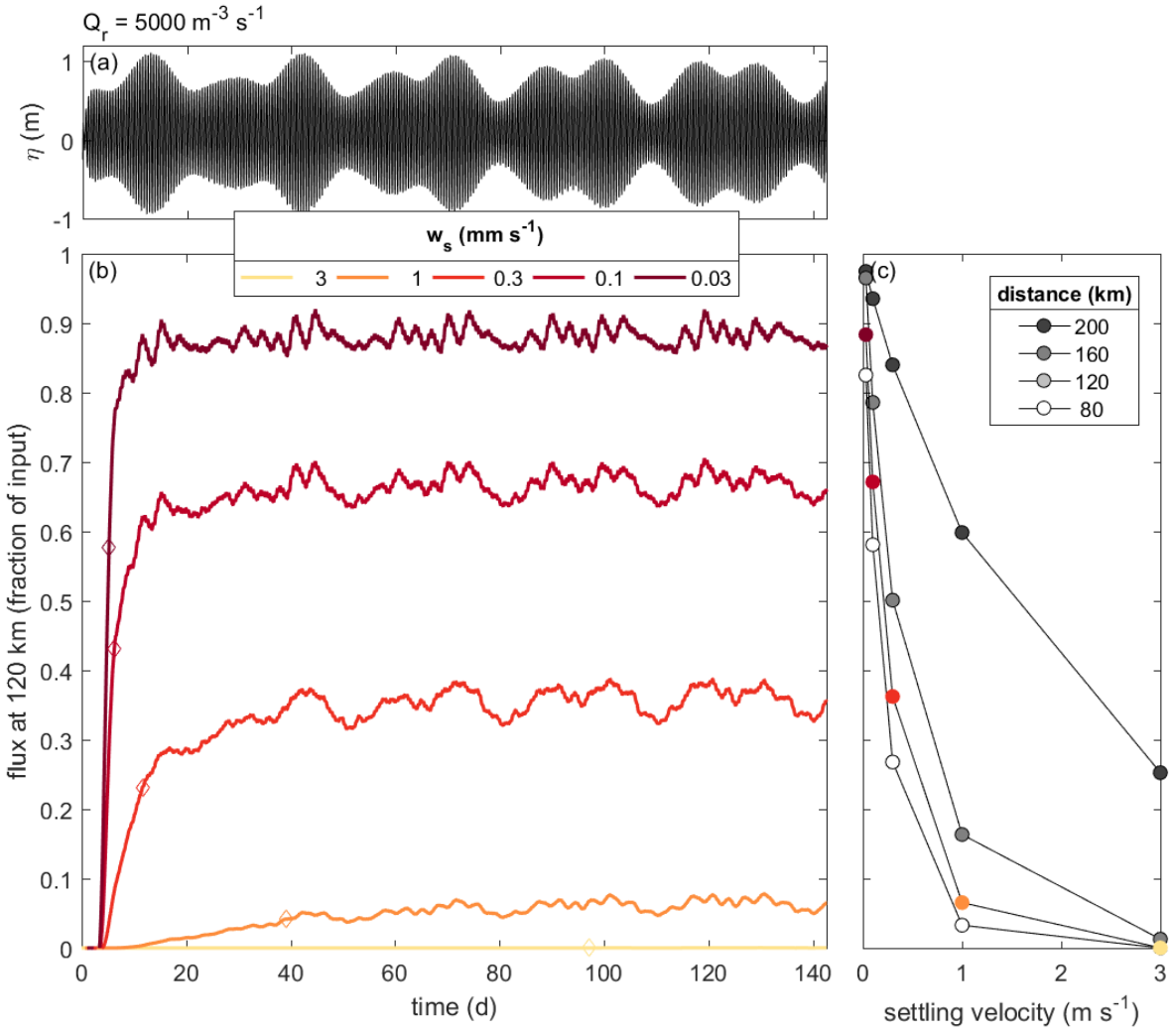

Figure 7. Sediment flux dependence on settling velocity. (a) Idealized tidal forcing for the constant discharge case of Q_r = 5000 m^3 s^{-1}. (b) Time series of tidally filtered sediment flux at 120 km (near Poughkeepsie) for sediment classes with settling velocity spanning 0.03 to 3 mm s^{-1}. (c) Sediment flux at the end of the simulation period for different locations along the river (80, 120, 160, 200 km) vs. settling velocity. The colored dots correspond with the full time series in (a).

In both the observations and the model, transport in the tidal river depends on the river discharge and the sediment settling velocity. To diagnose how these factors contribute, we ran idealized simulations over parameter space, applying the settling velocities from the realistic simulations (w_s = 0.01 and 0.2 mm s^{-1}) over a range of constant discharge cases (Q_r = 150, 300, 600, 2000, and 5000 m^3 s^{-1}) as well as testing a wider range of settling velocities (w_s = 0.03, 0.1, 0.3, 1 and 3 mm s^{-1}) for a constant discharge of 5000 m^{3}s^{-1}. The settling velocity dependence was

found to be independent of discharge, so a high discharge case was used to speed convergence toward equilibrium conditions.

The flux in the tidal river near Poughkeepsie (120 km) for an extended period with a constant discharge of 5000 $m^3 s^{-1}$ illustrates the dependence on settling velocity of both the timing and the magnitude of the seaward transport (Fig. 7). With the exception of the slowest settling sediment (3 mm s^{-1}), the flux time series at Poughkeepsie reached equilibrium values that was modulated by spring-neap variability in tidal amplitude. For the slowest settling sediment class (w_s = 0.03 mm s^{-1}), the equilibrium flux was almost 90% of the sediment input at the head of tide, and the flux relative to the input decreased as settling velocity increased, to 67%, 36%, 7%, and less than 1% for w_s = 0.1, 0.3, 1, and 3 mm s^{-1} respectively. The flux in each sediment class was greater at more landward cross-sections and less at more seaward locations, but at each position along the tidal river the flux decreased significantly for greater settling velocites (Fig. 7c).

The flux time series also show that the time required to reach the equilibrium depends on settling velocity (Fig. 7b). Using the time required to reach ($1-e^{-1}$) of the equilibrium flux for each class as a metric, the w_s = 0.03 mm s^{-1} sediment had a time scale of about 5 days while the 1 mm s^{-1} sediment was about 40 days or longer considering that the equilibrium flux had not been reached by the end of the simulation. A constant discharge from the Mohawk and Upper Hudson of 5000 $m^3 s^{-1}$ continuously for more than 4 months would never occur in nature, but it provides a means of quantify transport rates that are slow compared with the natural time scales of variability in discharge.

The transport time scale can also be characterized based on sediment age, which is tracked from the time sediment is input at the head of tide. Sediment age is compared with the advective time scale, or the age that a parcel of water moving through the system at the mean river velocity would have as a function of distance along the river (Fig. 8). For example, at 5000 $m^3 s^{-1}$ the advective time scale to reach Poughkeepsie (120 km) is just over 2 days and to reach the Battery (0 km) is about 7 days, as the mean velocity decreases as the cross-sectional area of the estuary increases toward the mouth. In contrast, at 150 $m^3 s^{-1}$ the transport time scale to

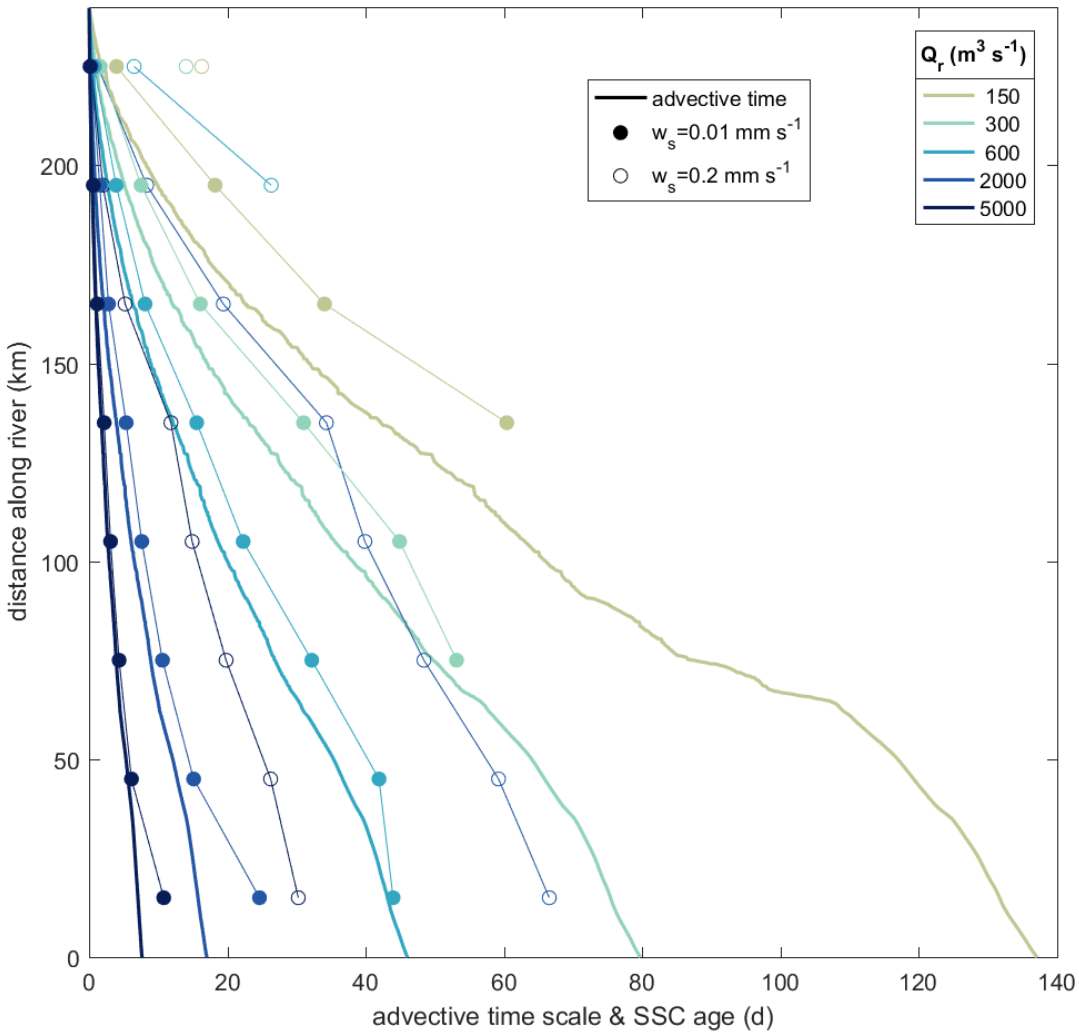

Figure 8. Advective time scales and sediment age. Solid lines are the advective time scale (distance/(Q_r/A)) vs. distance along the river for different constant discharge cases (150, 300, 600, 2000, 5000 m^3s^{-1}). Solid circles are the average age of suspended sediment with settling velocity = 0.01 mm s^{-1} vs. distance along the river for the same constant discharge cases, where suspended sediment age has been averaged in 30 km bins along the river. Open circles are the same but for settling velocity = 0.2 mm s^{-1}.

Poughkeepsie is almost 2 months and to the Battery is 4.5 months. Advective time scales calculated from tidally filtered velocities from the model results or more simply from the input river discharge divided by the cross-sectional area (Q_r/A) gave similar results.

Across the range of constant discharge cases, the age of suspended sediment parallels the advective time scale, each increasing with distance along the river (Fig. 8). Sediment age has been averaged over regular intervals along the river (in 30 km bins), and results are only shown

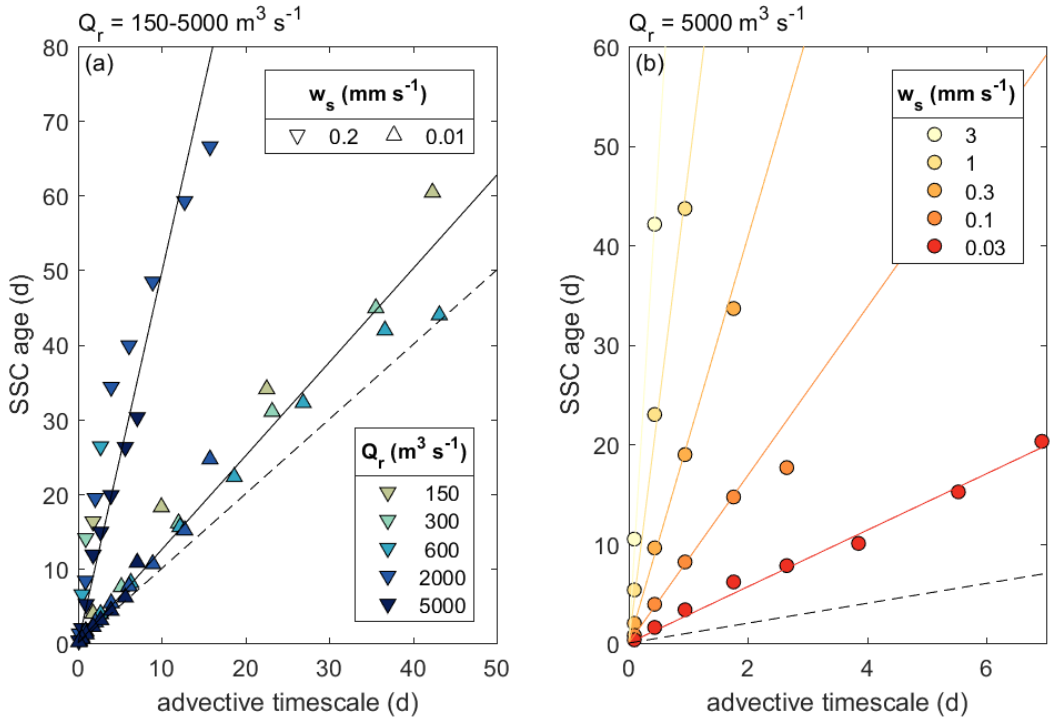

Figure 9. Advective time scale vs. suspended sediment age. (a) A range of constant discharge cases (150, 300, 600, 2000, 5000 m^3s^{-1}) with settling velocity = 0.01 and 0.2 mm s^{-1} (as in Fig. 8). (b) Constant discharge with 5000 m^3s^{-1} and a range of settling velocities (0.03, 0.1, 0.3, 1, 3 mm s^{-1}). Solid lines are best-fit slopes and dashed lines are a slope of 1. Suspended sediment age has been averaged in 30 km bins along the river, and only the bins with sufficient sediment to calculate a meaningful age at the end of each simulation are shown.

for regions with sufficient sediment at the end of the simulation to calculate a meaningful age. Faster settling, and therefore slower moving sediment classes are only found in the upper reaches of the river, as sufficient mass did not reach the lower reaches by the end of the simulations. For the more slowly settling sediment class in these cases (w_s = 0.01 mm s^{-1}), sediment age lagged the advective time scale for water only slightly. That lag increased significantly across all the discharge cases for the faster settling class (w_s = 0.2 mm s^{-1}).

Direct comparison the advective time scale with the sediment age for all the discharge cases results in a linear relationships that depend on settling velocity. Using the range of discharge cases, for the w_s = 0.01 mm s^{-1} the best-fit slope was 1.3 and for w_s = 0.2 mm s^{-1} the slope was 5.0. The slope represents the factor by which average suspended sediment age lags the

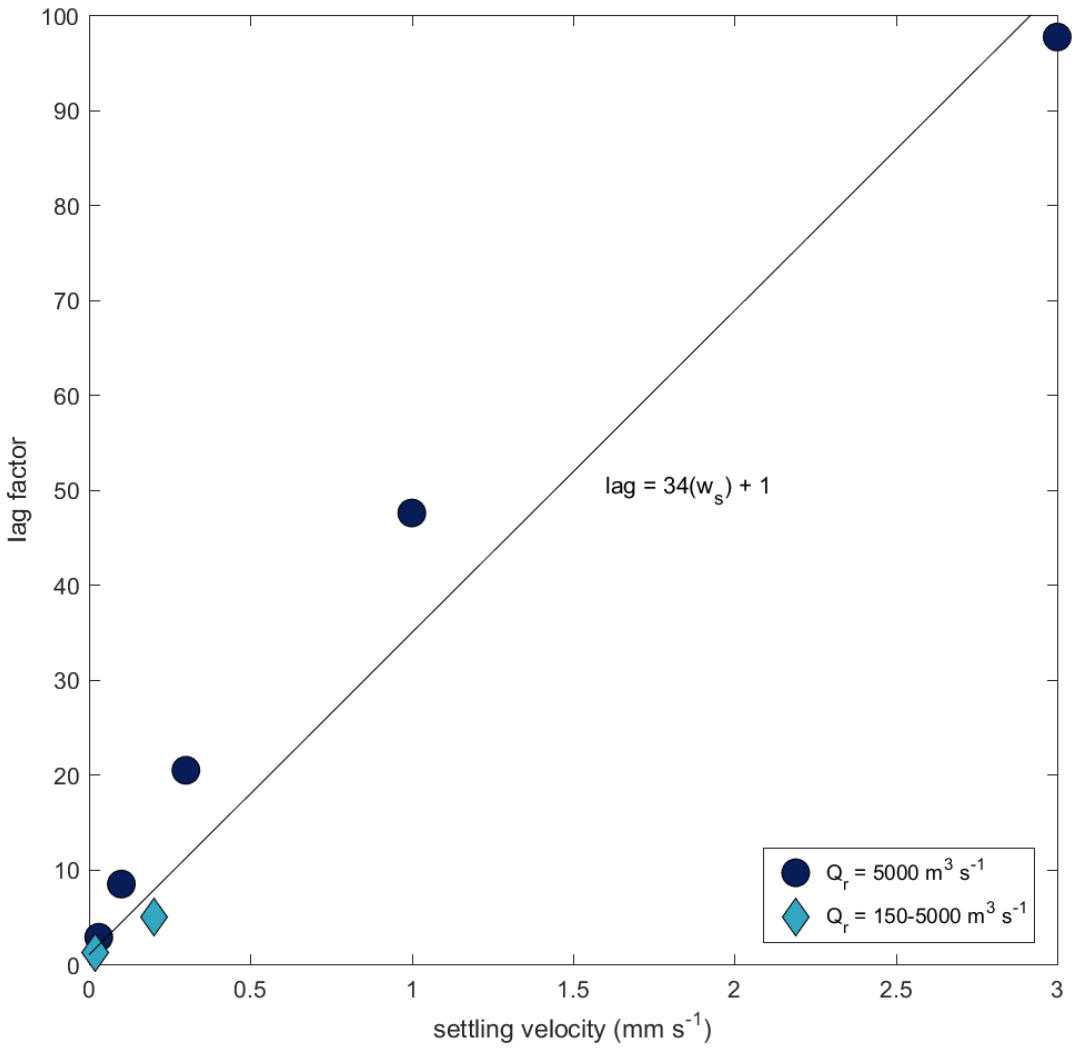

Figure 10. Suspended sediment lag factor vs. setting velocity. The lag factors are from the slope of the age vs. advective time scale in Figure 9, and represent factor by which sediment transport is slower than the water volume transport.

advective time scale (Fig. 9a), so we can write a scaling for mean age of suspended sediment (a_{ssc}) based on those factors:

$$a_{ssc} = \lambda_{ws} t_{adv} \qquad (1)$$

where λ_{ws} is the slope or lag factor and t_{adv} is the advective time scale for water. The same linear scaling holds across the wider range of settling velocities used in the Q_r = 5000 m^3 s^{-1} case (Fig. 9b). For w_s = 0.03 mm s^{-1}, the lag factor of 2.8 represented the sediment age well over the entire

tidal river at the end of the simulation. For the 3 mm s^{-1} sediment, the transport rate was substantially slower, with a best-fit slope is 98. As noted previously, the faster settling sediment classes were limited to the upper river due to their high rates of deposition (Fig. 7) and slow rates of transport (Fig. 9b), so the slope estimates are limited to a few data points and are not well constrained. The spatial heterogeneity of the Hudson River domain introduces variability in the detailed hydrodynamics and sediment transport, and consequently in sediment age distribution, but the linear relationship between the advective time scale and sediment age does not appear to depend on distance along the river.

Based on the idealized model cases spanning discharge and settling velocity parameter space, we evaluate the relationship between settling velocity and the lag in sediment transport rate, or specifically the suspended sediment age relative to the advective time scale (Fig. 10). The best-fit slope considering all the cases results a lag factor that is 34 times the settling velocity (in mm s^{-1}). This regression is influenced by the fast settling sediment classes (3 mm s^{-1} for Q_r = 5000 m^3s^{-1} and 0.2 mm s^{-1} for the wider range of Q_r cases) that are less well constrained due to the finite simulation period and limited transport extent, so this best-fit may in fact underestimate the effective lag in sediment transport, and correspondingly in sediment age. For example, the 0.3 and 1.0 mm s^{-1} sediment classes had lag factors of 20 and 48 respectively for Q_r = 5000 m^3 s^{-1}, while the regression would predict values of 10 and 34. Still, the idea that sediment transport scales with the river velocity but is lagged by a factor that depends linearly on settling velocity appears to be robust and a useful conceptual framework for characterizing sediment age in the tidal river.

4.3 Sediment age distribution

The average sediment age for suspended sediment is well described by the advection time scale and settling velocity, but the bin averaging by distance along the river masks spatial heterogeneity associated with the bathymetry. In the deeper channel where flow velocity and stress are greater, suspended sediment age is less than it is in more depositional, retentive areas on lateral shoals at a similar distance from the head of tide (Fig. 11). Similarly, the age of new sediment that deposited on the bed increases with distance along the river and has lateral structure corresponding with the bathymetry. As with suspended sediment, bed age is greater in

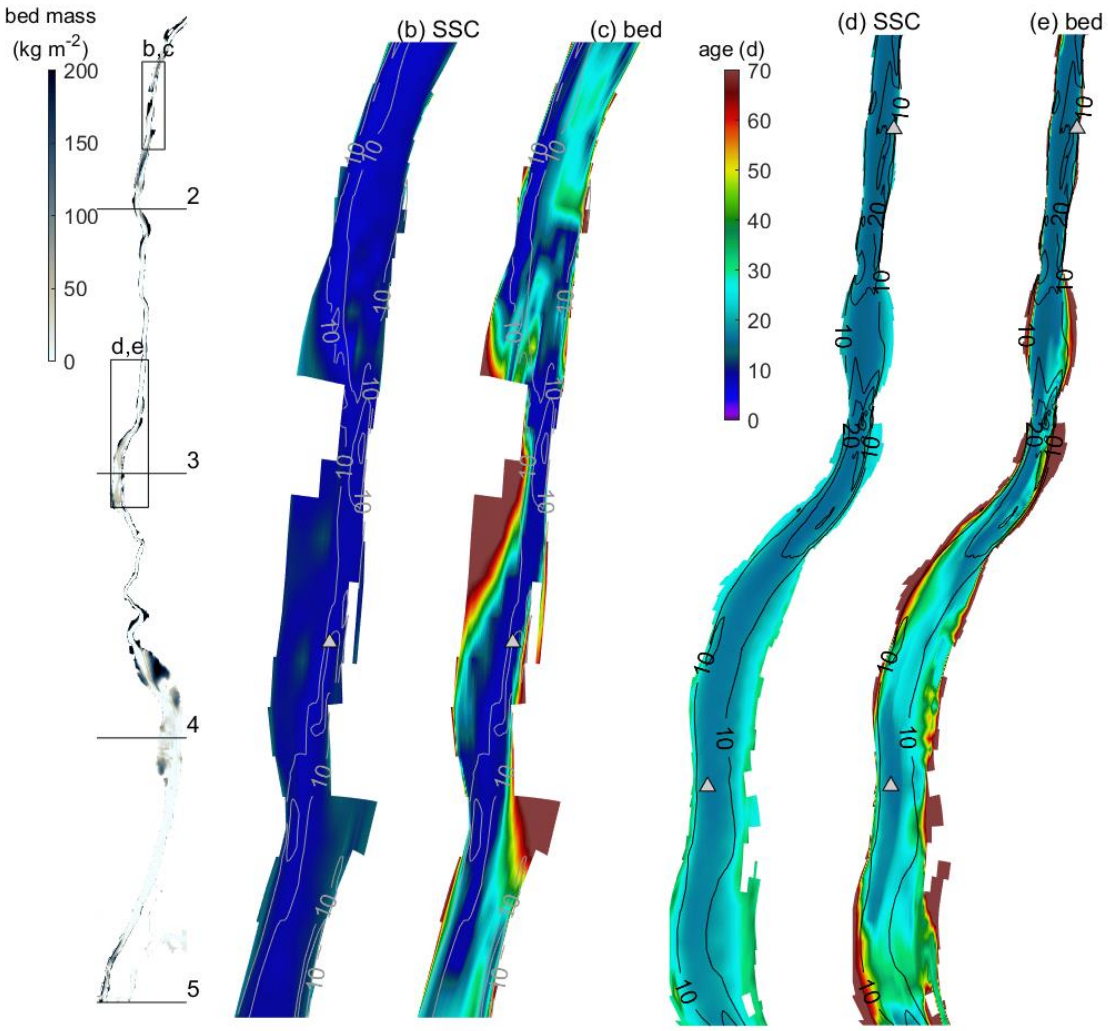

Figure 11. Maps of suspended and bed sediment age for settling velocity of 0.1 mm s^{-1}. The results are from the end of a simulation with constant discharge of 5000 m^3s^{-1} (145 day duration). (a) Mass distribution of sediment from river inputs. (b,c) Maps of suspended sediment age and bed sediment age near Tivoli (as in Fig. 6a). (d,e) Maps of suspended sediment age and bed sediment age near Poughkeepsie and Newburgh (as in Fig 6b). Bathymetry contours are plotted along with locations of observations.

depositional regions at the sides of the channel, while river input sediment that is on the bed in the channel has on average been introduced to the system more recently.

At any location along the river, sediment on the bed is older than sediment in the water column (Fig. 11). Suspended sediment in each size class advects seaward at the mean velocity set by the river discharge times the lag factor for its settling velocity, and that scaling predominantly determines the age of suspended sediment at a given location. Some of that

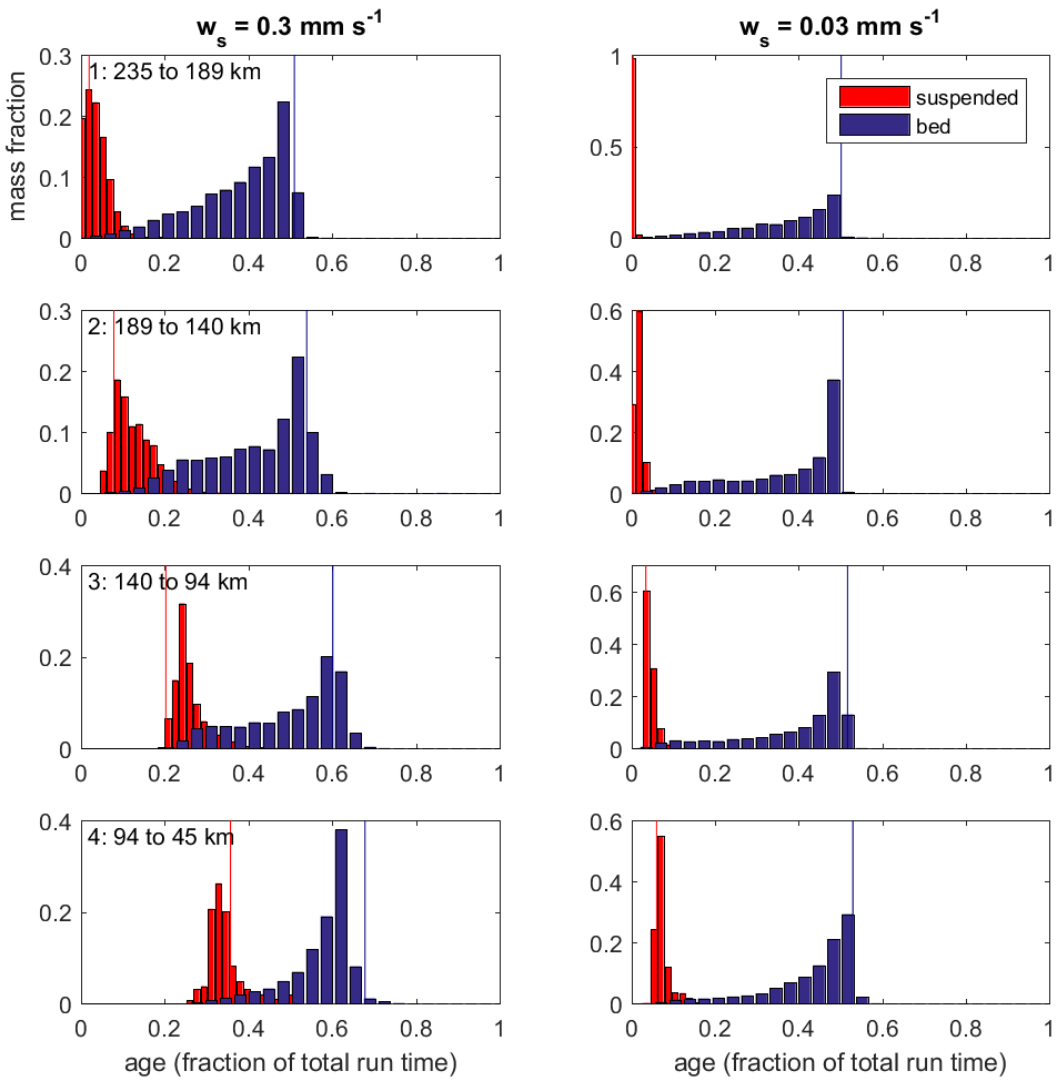

Figure 12. Histograms of suspended and bed sediment age as a function of distance along the river (averaged in ~45 km bins) and settling velocity (0.3 and 0.03 mm s^{-1} sediment classes shown). Vertical lines are the time scales for suspended sediment (Eqn. 1, red lines) and bed sediment age (Eqn. 2, blue lines).

suspended sediment deposits on the bed, and that newly deposited sediment mixes with any older, previously deposited sediment that is already there. As reminder, the age calculations are focusing only on new sediment input from the tributaries, independent f the sediment classes on the bed at the start of the simulation. The age of the newly input sediment that is on the bed then is the weighted average of the newly delivered and previously deposited sediment, and the bed sediment continues to age in place through the simulation. Thus a scaling for the age of river input sediment on the bed (a_{bed}) at a given location is the average of the simulation time (the

oldest sediment at this location, which came into the domain at the start of the simulation) and the advective time scale for that sediment class (the youngest sediment, which most recently arrived)

$$a_{bed} = \frac{1}{2}(\lambda_{ws} t_{adv} + t_{sim}) \qquad (2)$$

where t_{sim} is the duration of the model run.

The age distribution of the river input sediment in suspension and on the bed can be represented quantitatively with histograms for discrete regions of the tidal river (Fig. 12). Sediment ages have been normalized to the total simulation period, because as noted above the average age in depositional bed regions continues to grow with time. Two settling velocities illustrate common patterns among the sediment classes, including that age of both suspended and bed sediment at a given location is greater for greater settling velocity. The time scales for the age of suspended sediment (Eqn. 1) and on the bed (Eqn. 2) correspond reasonably well with the center of the age distributions in the model with complex bathymetry. The lag factors to calculate the age scale for the sediment classes were from the regression to settling velocity (Fig 10). Tidal processes and bathymetric variability lead to dispersion of the sediment pulse as it moves seaward, with greater spread in age for the faster settling sediment, but generally the simple scaling based on settling velocity and river discharge represents the middle of the suspended sediment age distribution. For bed sediment, the scaling represents the mode of the distribution reasonably well, but the tail of the distribution is skewed toward younger ages. The histograms of the bed conditions combine both highly depositional regions that continuously accumulate sediment through the simulation and regions of that are more erosional and have only recent or ephemeral deposition. The mode represents the depositional regions, while the tail are the more dynamic channel regions.

The constant discharge cases demonstrate the mean age of suspended sediment can be calculated as a function of discharge, settling velocity, and distance along the river, recognizing that some spatial variance is introduced by the realistic bathymetry. Because the sediment transport rates were much slower than the mean river velocity, even for the high discharge case (5000 $m^3 s^{-1}$, U_r = 0.3-2 m s^{-1}) the sediment fluxes in the tidal river took weeks to months to

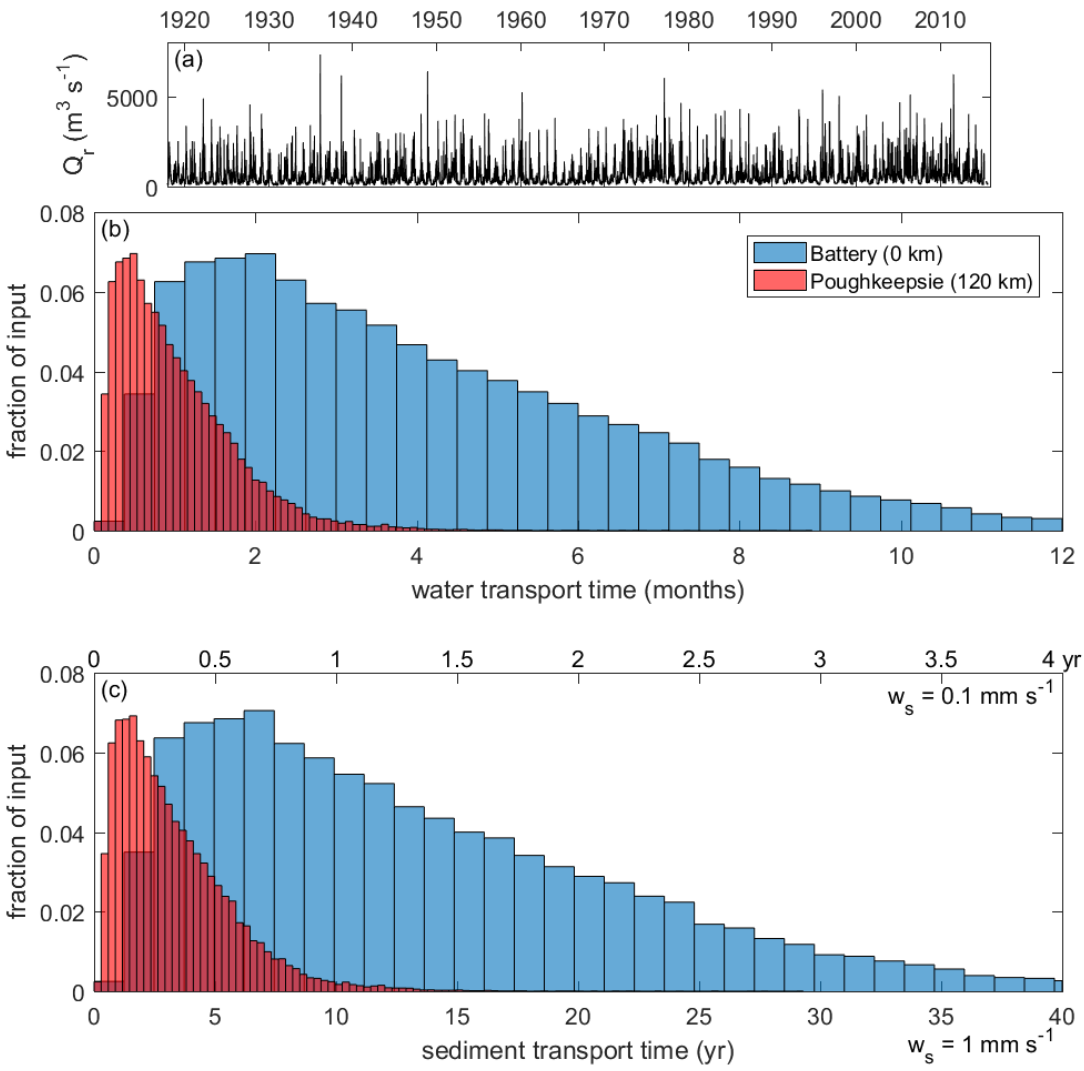

Figure 13. Age distributions based on advective time scales and historical discharge. (a) Discharge time series based on observations of the Mohawk (at Cohoes) and Upper Hudson (at Waterford) multiplied by 1.4 to represent tributary inputs to the Lower Hudson. (b) Distribution of advective time scales for water to travel from the head of tide (240 km) to Poughkeepsie (120 km) and the Battery (0 km). (c) Distribution of suspended sediment ages at the same locations based on the discharge time series and lag factors for settling velocities of 0.1 mm s^{-1} (top axis labels) and 1 mm s^{-1} (bottom axis labels). Note water transport time is plotted in months and sediment ages in years.

equilibrate with the input for sediment with settling velocities greater than ~0.5 mm s^{1}. High river discharge periods typically last days (storm events) to weeks (spring freshet), as river velocity decreases the sediment transport rate does as well, so the time to equilibrium increases. For most of the sediment most of the time, the system is far from equilibrium, an evaluation of sediment age under realistic forcing has to take into account the temporal variability in river

discharge at the seasonal to interannual scale, as well as the differences in transport rate by sediment size class.

The time series of river discharge from observations at gauges on the Mohawk and Upper Hudson dating back to 1917 is used to represent the temporal variability in forcing (Fig. 13). To account for inputs from tributaries flowing directly into the lower Hudson that were ungauged for most of this period, the Mohawk and Upper Hudson discharge is multiplied by 1.4 based on the ratio of watershed areas and observations at Poughkeepsie [*Wall et al.*, 2008]. For any location along the river, the discharge time series and the average cross-sectional area landward of that point can be used to calculate a distribution of advective time scales for water (Fig. 13b). Near Poughkeepsie (120 km), above which is almost always fresh, the mode of the advective time scale is about 0.5 months, with a skewed distribution toward longer time scales of a few months during low discharge periods. Similarly, the travel time for water to the Battery (0 km) has a mode of 2 months and a tail extending to more than 1 year.

As both the idealized and realistic model results show, the age distribution of sediment associated with a particular discharge event depends both on settling velocity and the specific time history of the river discharge. The input of sediment to the tidal river is highly nonlinear (Fig. 3), but the model and observations indicate that sediment transport scales linearly with discharge, so for a sufficiently long integrating time scale we can use the discharge time series to represent the sediment travel time statistically. The sediment transport time depends simply on the transport time for water (Fig. 13b) and the lag factor for that settling velocity (Fig. 10). For w_s = 1 mm s^{-1}, the lag factor of about 40 corresponds with sediment transport times from the tidal limit (240 km) to Poughkeepsie (120 km) of 1.5 years (mode) to 5-10 years or more in the tail of the distribution. The lag factor scales linearly with w_s, so for 0.1 mm s^{-1} sediment transport times are a factor of 10 less, in the range of a few months to a year. Transport times to the Battery are about 5 times as long as to Poughkeepsie. For w_s = 1 mm s^{-1}, the mode is about 7 years and the tail extends out several decades, while for w_s = 0.1 mm s^{-1} the characteristic transport time scales are 0.5 to 5 years. Note that the conceptual model was developed based on the sediment transport rates in the fresh tidal river, and therefore likely represents a lower bound on transport time scales once sediment reaches the saline estuary. Geochemical and physical observations in the lower Hudson estuary have found significant landward transport and recycling of sediment from

New York Harbor [*Feng et al.*, 1999; *Geyer et al.*, 2001], as the sediment trapping by estuarine processes makes seaward transport less efficient and the system more retentive than in the fresh tidal river. Additionally, flocculation in the estuary will shift some of the finer sediment into faster settling flocs, effectively increasing the transport time for some of the sediment that moved seaward through the tidal river more rapidly as individual particles.

4.4 Advection, deposition, and settling velocity

In addition to the lag in the sediment transport speed compared with the river velocity, the model results show that the loss rate due to deposition, and thus the equilibrium transport rate as a function of distance along the river, depends on settling velocity (Fig. 7). A simple conceptual model can be used to characterize the rate of sediment loss along the tidal river, where the decrease in sediment transport is due to sediment settling in depositional areas. For a discrete segment of the river at equilibrium flow conditions, the sediment mass balance can be written as

$$Q_r C_{out} = Q_r C_{in} - C_{in} w_s B \Delta x \qquad (3)$$

where Q_r is the river discharge, w_s is the settling velocity, B is the channel width, Δx is the length of the channel segment, and C_{in} and C_{out} are sediment concentrations at the upstream and downstream ends. Q_r is uniform so spatial gradients in flux are due to a decrease in sediment concentration with distance along the river due to settling, the third term in (3). This is the same as an advection-reaction model with the time constant for the reaction rate $k = w_s/H_s$, where H_s is the water depth where settling occurs. In the limit of small Δx the solution to (3) can be written as

$$C(x) = C_0 \exp(-\frac{w_s}{H_s} t_{adv} \delta) \qquad (4)$$

where C_0 is the input concentration, x is the distance from the head of tide, and $t_{adv}(x)$ is the advective times scale for sediment transport, which is nominally $x/(Q_r/A)$. We have included a duty cycle factor δ because settling occurs predominantly at slack tide, which represents only a small fraction of the tidal cycle.

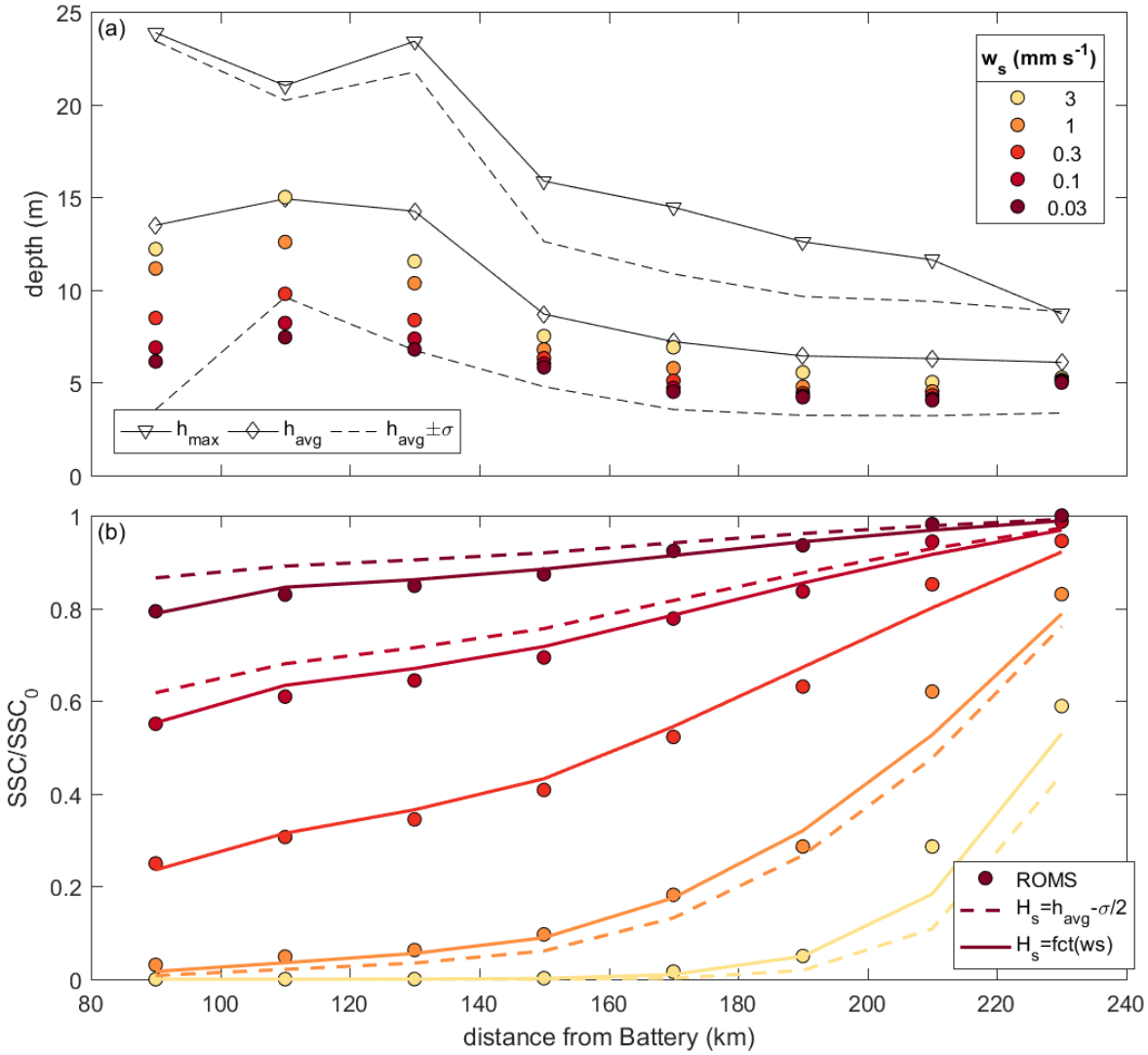

Figure 14. Modeling the decrease in sediment flux along the river by advection and settling. (a) In 30 km segments along the river, mass-weighted average of the water depth where sediment deposited by sediment settling velocity classes. Also shown is the mean thalweg depth (h_{max}), the mean depth (h_{avg}), the mean depth ± 1 standard deviation of the depth (σ) in each 30 km segment. (b) Average SSC with distance relative to the input at the head of tide (SSC_0). Also plotted are advection-reaction model (Eqn. 4) results with the settling depth $H_s = h_{avg} - 0.5*\sigma$, and with $H_s = h_{avg} - f*\sigma$, where f varies linearly between 0 and 1 for the settling velocity classes from 3 to 0.03 mm s^{-1}.

The applicability of the conceptual model can be tested by plotting at the end of the constant discharge simulation (Q_r =5000 m^3 s^{-1}) the sediment concentration distribution along the river relative to the input concentration at the tidal limit (SSC_0) (Fig. 14). The advection-reaction model depends on the choice of an appropriate settling water depth H_s. In the Hudson, both the

mean and thalweg depths increase with distance downriver, with the thalweg 1.5 to 2 times the average depth. Deposition occurs preferentially in shallower regions on the edges of the river (Figs. 6 and 11), and this is reflected in the mass-weighted average depth of where newly input river sediment has deposited (Fig. 14a). The average depth of deposition was even shallower the slower settling size classes. The longer that sediment remains in the water column each tide, the more disperses into low energy regions at the edges of the river where it can then deposit. In contrast, the faster settling size classes remained predominantly in deeper regions closer to the main flow of the channel.

First we apply the advection-reaction model using a single settling depth for all sediment size classes. Based on the average depth of depositional regions (Fig. 14a), we set H_s to be halfway between the average depth and the average depth minus 1 standard deviation: $H_s = h_{avg} - 0.5*\sigma$. The duty cycle ∂ was set to 1/9, which corresponds to approximately 40 minutes of settling time during each slack tide, keeping in mind this is not well constrained and has a similar effect on the model as H_s. Using the range of settling velocities and the advective time scale for water, we find that the simple advection-reaction model explains much of the variation in transport efficiency among the sediment size classes (Fig. 14b). Alternatively, we can try to account for the spatial difference in where sediment settles by size class, with finer particles dispersing into shallower regions at the river edges. For simplicity, we allow H_s to vary linearly among the sediment size classes, from $H_s = h_{avg}$ for w_s = 3 mm s^{-1} to $H_s = h_{avg} - \sigma$ for w_s = 0.03 mm s^{-1}. This variation was set empirically based on the sediment deposition patterns in the ROMS model (Fig. 14a), but it is consistent with our conceptual understanding of the system and accounts for much of the residual error compared with using a single value for H_s for all the size classes.

5. SUMMARY AND DISCUSSION

5.1 Key results

The Hudson watershed, tidal river, and estuary has a fairly extensive observational record with which we can begin to characterize the magnitude and time scales of terrestrial material fluxes to the coastal ocean. Discrepancies between the sediment discharge from tributary rivers and the seaward fluxes measured in the lower tidal river indicate that sediment delivery is

significantly altered by the tidal river, with both deposition and delay in sediment discharge relative to inputs. The discrepancy arises from a difference in the dependence on river discharge of the watershed inputs and the transport in the tidal river. The watershed loading is highly non-linear, with a discharge dependence that is nearly cubic. In contrast, the seaward flux in the tidal river is approximately linear with discharge (Fig. 3). Consequently, while sediment delivery occurs primarily during the largest discharge event of the year or the decade, the transport in the tidal river does not scale up as rapidly, and much of that new sediment remains on the bed of the tidal river for months to years after the event.

We used the model with realistic bathymetry but idealized forcing to characterize how transport in the tidal river depends on the forcing (primarily river discharge) and sediment characteristics (primarily settling velocity). To quantify time scales of sediment transport, we adapted the tracer age model to apply to sediment both in the water column and on the bed. Both observations and the model show that suspended sediment input with discharge events advects seaward at a rate slower than the mean river velocity. With the model, we find that the age of suspended sediment newly input to the tidal river was well characterized by the advective time scale for water multiplied by a lag factor that scaled linearly with settling velocity. The wide range of settling velocities of particles in the environment then correspond with an equally wide range of transport time scales. Applying the suspended sediment age scaling to the observed time series of river discharge in the Hudson results in transport time scales through the tidal river and to the ocean of years for fine silt (w_s = 0.1 mm s^{-1}) to decades for coarse silt (w_s = 1 mm s^{-1}) (Fig. 13).

In addition to the timing of sediment delivery to the ocean, settling velocity also affects the magnitude through the fraction of sediment that is retained in the tidal river. Transport efficiency decreases with settling velocity, and a simple advection-reaction equation can represent the decrease in SSC and transport due to settling with distance along the river. Deposition occurs primarily on lower energy shoals and side embayments, while the channel bed is generally coarser and more dynamic. The sorting of particles along the tidal river by preferential loss of faster settling sediment is consistent with observed bed composition distribution [*Nitsche et al.*, 2007].

5.2 Settling velocity and sediment transport

The model results highlight the extreme sensitivity of the sediment transport efficiency to settling velocity. Settling velocity of discrete particles corresponds with grain size, although flocculation can greatly increase the settling velocity of small particles, particularly in the saline estuary. In the tidal river at Poughkeepsie, the suspended sediment is predominantly fine (< 63 μm) [*Wall et al.*, 2008], but the particle settling velocities range from 3 mm s^{-1} for coarse silt to less than 0.01 mm s^{-1} for clay. As noted above, the suspended sediment observations at Poughkeepsie from *Wall et al.* [2008] are consistent with the simultaneous presence of a washload at the lower end of this settling velocity range and a particle population at the upper end of the range that resuspends and settles with the tides.

Previous analysis of primary particle size of suspended sediment in the upper saline estuary (Haverstraw Bay) found a bi-modal distribution, with peaks at <5 μm and 22-63 μm [*Menon et al.*, 1998]. Characterizing these ranges as "fine" and "coarse", that study found that the ratio of fine-to-coarse increased from about 1 near the head of tides to about 2 in the lower tidal river. The clay size range (<2 μm) represented 11% of the particles in samples from the Mohawk and Upper Hudson, but the clay fraction increased to 26% at Poughkeepsie, suggesting deposition of coarser silt along the upper tidal river. The increased prevalence of finer particles in the suspended sediment is consistent with the greater fraction of mud with distance from the head of tide [*Nitsche et al.*, 2007].

Direct measurements of settling velocity measurements remain a major observational challenge. Estimates of settling velocity made by assuming fits to a Rouse profile found a wide range of values in the lower ETM of the saline estuary, ranging from 0.6 to 6 mm s^{-1} with a characteristic value of 2 mm s^{-1} [*Orton and Kineke*, 2001]. The Rouse approach can effectively characterize homogenous particle populations in steady flow, but is difficult to constrain if there are multiple, disparate sediment size classes at once. Primary particle size distributions measured in the laboratory or in-situ can characterize spatial and temporal trends in the sediment composition but the connection to settling velocity depends on other characteristics of the suspended material (e.g., mineral and organic composition) and the flow (turbulence, salinity). Given the sensitivity of the transport efficiency and age calculations to settling velocity, a better characterization of the settling velocity distribution in the environment would be the most

effective means of reducing uncertainty in the characterization of sediment fluxes and in sediment transport modeling.

5.3 Time scales of transport

High discharge periods deliver sediment to the upper tidal river and also correspond with increased suspended sediment concentrations in the saline estuary [*Geyer et al.*, 2001]. During the spring freshet, deposition increases in the lower estuary near the Battery, and as the discharge decreases in the months that follow this sediment is eroded and sedimentation increases 20 km landward in the lower ETM [*Woodruff et al.*, 2001]. While it is tempting to assume the increased sediment concentrations and deposition rates in the estuary are due to the increased sediment load from the watershed, the observational and model results indicate otherwise. In addition to the increased supply, high discharge conditions increase bed stress and mobilize sediment in the tidal river and estuary thereby increasing the total seaward sediment transport, although little of that sediment came in with the discharge event. In particular, seaward advection of the salinity intrusion exposes regions of the estuary that were previously salinity stratified and trapping sediment to the greater bed stresses and greater erosion rates of a tidal fresh regime [*Ralston et al.*, 2013]. Thus, in a system like the Hudson with an extensive tidal fresh region, much of the seasonal increase in suspended sediment in the estuary is due to remobilization rather than new inputs from the watershed.

The scaling of sediment age with mean river velocity and particle settling velocity suggests that rather than the days to weeks of a high discharge event, the time scales for sediment delivery to the estuary are years to decades (Fig. 13). The suspended sediment age is highly variable, depending linearly on both on the river discharge (1-2 orders of magnitude variability) and settling velocity (at least 3 orders of magnitude variability). The age of bed sediment is even more heterogeneous, including both dynamic channel bed that may have ephemeral deposits of new sediment and more depositional regions that continuously accumulate sediment and grow in average age. Sediment age, which measures how long sediment is retained in the tidal river or estuary, has implications for the fate of organic constituents and metals that are preferentially associated with particles. For particulate organic matter, the amount of consumption and transformation that occurs in an estuary increases as the length and the residence time of the estuary increases [*Middelburg and Herman*, 2007]. The results here suggest that the length and

residence time of the tidal fresh river also could be an important factor affecting the composition of terrestrial organic matter that reaches the estuary. Observations from over 3 years in the tidal fresh Hudson found that particulate organic carbon concentration depended more on processes in the tidal river than the external loading from tributaries, consistent with a long residence time and extensive processing of particles entering from the watershed [*Findlay et al.*, 1991]. Similarly, estuaries with longer residence times tend to be more heterotrophic, which affects the rate of degassing of carbon dioxide to the atmosphere [*Cai*, 2011]. Much of the organic matter consumed in estuaries is thought to be produced by adjacent wetlands or by in-situ phytoplankton blooms, but the quantity and composition of the organic matter coming off the land will depend on how it travels through the tidal river.

Time scales of recovery for contaminated sediments also depend on sediment transport time scales. As with many urbanized rivers, the Hudson has a long history of industrialization and associated contaminant inputs, including PCBs and heavy metals. A major source of PCBs was from the Upper Hudson River, so the contaminants are distributed along the length of the tidal river and estuary. PCB concentration chronologies reconstructed from cores along the tidal fresh Hudson and in the estuary give recovery time scales of several years to more than a decade based on the *e*-folding of the concentration decrease [*Bopp and Simpson*, 1989; *Rodenburg and Ralston*, 2017]. Sediment cores from depositional regions integrate over the temporal variability of sediment loading to better characterize the long-term adjustment time scales, but more such studies are needed to account for the spatial heterogeneity in sedimentation and poor constraints on contaminant inputs. As with all aspects of sediment transport, contaminant fates are also highly dependent on particle size because the greater surface-area-to-volume of fine particles increases the adsorption of metals. For example in the Hudson the maximum concentrations of copper, zinc, cadmium and lead were found in the ETM associated with particles < 2 μm [*Menon et al.*, 1998]. The results here suggest that such fine sediment moves relatively efficiently through the tidal river but may become more readily retained if it becomes associated with flocs when it reaches the saline estuary. The issue highlights the intrinsic coupling between settling velocity and residence time in the tidal river and estuary, and the critical importance of refining our understanding of both.

Data access

Data generated during this project, including observations and model results, are available upon request from David Ralston (dralston@whoi.edu).

References

Abood, K. A. (1974), Circulation in the Hudson Estuary, *Ann. N. Y. Acad. Sci.*, *250*(1), 39–111, doi:10.1111/j.1749-6632.1974.tb43895.x.

Benoit, G., E. X. Wang, W. C. Nieder, M. Levandowsky, and V. T. Breslin (1999), Sources and history of heavy metal contamination and sediment deposition in Tivoli South Bay, Hudson River, New York, *Estuaries*, *22*(2), 167–178, doi:10.2307/1352974.

Bokuniewicz, H. J., and J. M. Ellsworth (1986), Sediment budget for the Hudson system, *Northeast. Geol.*, *8*(3), 156–164.

Bopp, R. F., and H. J. Simpson (1989), Contamination of the Hudson River: The sediment record, *Contam. Mar. Sediments Assess. Remediat.*, 401–416.

Bowen, M. M., and W. R. Geyer (2003), Salt transport and the time-dependent salt balance of a partially stratified estuary, *J. Geophys. Res.*, *108*(C5), 3158, doi:10.1029/2001JC001231.

Cai, W.-J. (2011), Estuarine and Coastal Ocean Carbon Paradox: CO2 Sinks or Sites of Terrestrial Carbon Incineration?, *Annu. Rev. Mar. Sci.*, *3*(1), 123–145, doi:10.1146/annurev-marine-120709-142723.

Chillrud, S. N., R. F. Bopp, J. M. Ross, D. A. Chaky, S. Hemming, E. L. Shuster, H. J. Simpson, and F. Estabrooks (2004), Radiogenic Lead Isotopes and Time Stratigraphy in the Hudson River, New York, *Water Air Soil Pollut. Focus*, *4*(2), 469–482, doi:10.1023/B:WAFO.0000028372.87703.b7.

Deleersnijder, E., J.-M. Campin, and E. J. M. Delhez (2001), The concept of age in marine modelling: I. Theory and preliminary model results, *J. Mar. Syst.*, *28*(3–4), 229–267, doi:10.1016/S0924-7963(01)00026-4.

Delhez, E. J. M., J.-M. Campin, A. C. Hirst, and E. Deleersnijder (1999), Toward a general theory of the age in ocean modelling, *Ocean Model.*, *1*(1), 17–27, doi:10.1016/S1463-5003(99)00003-7.

Downing-Kunz, M. A., and D. H. Schoellhamer (2015), Suspended-Sediment Trapping in the Tidal Reach of an Estuarine Tributary Channel, *Estuaries Coasts*, *38*(6), 2198–2212, doi:10.1007/s12237-015-9944-4.

Dunne, T., L. A. K. Mertes, R. H. Meade, J. E. Richey, and B. R. Forsberg (1998), Exchanges of sediment between the flood plain and channel of the Amazon River in Brazil, *Geol. Soc. Am. Bull.*, *110*(4), 450–467, doi:10.1130/0016-7606(1998)110<0450:EOSBTF>2.3.CO;2.

Ensign, S. H., G. B. Noe, and C. R. Hupp (2014), Linking channel hydrology with riparian wetland accretion in tidal rivers, *J. Geophys. Res. Earth Surf.*, *119*(1), 2013JF002737, doi:10.1002/2013JF002737.

Feng, H., J. K. Cochran, D. J. Hirschberg, and R. E. Wilson (1998), Small-Scale Spatial Variations of Natural Radionuclide and Trace Metal Distributions in Sediments from the Hudson River Estuary, *Estuaries*, *21*(2), 263–280.

Feng, H., J. K. Cochran, and D. J. Hirschberg (1999), 234Th and 7Be as tracers for the transport and dynamics of suspended particles in a partially mixed estuary, *Geochim. Cosmochim. Acta*, *63*(17), 2487–2505, doi:10.1016/S0016-7037(99)00060-5.

Findlay, S., M. Pace, and D. Lints (1991), Variability and transport of suspended sediment, particulate and dissolved organic carbon in the tidal freshwater Hudson River, *Biogeochemistry*, *12*(3), 149–169, doi:10.1007/BF00002605.

Geyer, W. R., J. D. Woodruff, and P. Traykovski (2001), Sediment Transport and Trapping in the Hudson River Estuary, *Estuaries*, *24*(5), 670–679.

Godin, G. (1999), The Propagation of Tides up Rivers With Special Considerations on the Upper Saint Lawrence River, *Estuar. Coast. Shelf Sci.*, *48*(3), 307–324, doi:10.1006/ecss.1998.0422.

Goodbred Jr., S. L., and S. A. Kuehl (1998), Floodplain processes in the Bengal Basin and the storage of Ganges–Brahmaputra river sediment: an accretion study using 137Cs and 210Pb geochronology, *Sediment. Geol.*, *121*(3–4), 239–258, doi:10.1016/S0037-0738(98)00082-7.

Haidvogel, D. B. et al. (2008), Ocean forecasting in terrain-following coordinates: Formulation and skill assessment of the Regional Ocean Modeling System, *J. Comput. Phys.*, *227*(7), 3595–3624, doi:10.1016/j.jcp.2007.06.016.

Hoitink, A. J. F., and D. A. Jay (2016), Tidal river dynamics: Implications for deltas, *Rev. Geophys.*, *54*(1), 2015RG000507, doi:10.1002/2015RG000507.

Klingbeil, A. D., and C. K. Sommerfield (2005), Latest Holocene evolution and human disturbance of a channel segment in the Hudson River Estuary, *Mar. Geol.*, *218*(1–4), 135–153, doi:10.1016/j.margeo.2005.02.026.

McHugh, C. M. G., S. F. Pekar, N. Christie-Blick, W. B. F. Ryan, S. Carbotte, and R. Bell (2004), Spatial variations in a condensed interval between estuarine and open-marine settings: Holocene Hudson River estuary and adjacent continental shelf, *Geology*, *32*(2), 169–172, doi:10.1130/G20150.1.

Menon, M. G., R. J. Gibbs, and A. Phillips (1998), Accumulation of muds and metals in the Hudson River estuary turbidity maximum, *Environ. Geol.*, *34*(2), 214–222, doi:10.1007/s002540050273.

Mercier, C., and E. J. M. Delhez (2007), Diagnosis of the sediment transport in the Belgian Coastal Zone, *Estuar. Coast. Shelf Sci.*, *74*(4), 670–683, doi:10.1016/j.ecss.2007.05.010.

Middelburg, J. J., and P. M. J. Herman (2007), Organic matter processing in tidal estuaries, *Mar. Chem.*, *106*(1–2), 127–147, doi:10.1016/j.marchem.2006.02.007.

Milliman, J. D., and K. L. Farnsworth (2013), *River Discharge to the Coastal Ocean: A Global Synthesis*, Cambridge University Press.

Milliman, J. D., S. Huang-ting, Y. Zuo-sheng, and R. H. Mead (1985), Transport and deposition of river sediment in the Changjiang estuary and adjacent continental shelf, *Cont. Shelf Res.*, *4*(1–2), 37–45, doi:10.1016/0278-4343(85)90020-2.

Nash, D. B. (1994), Effective sediment-transporting discharge from magnitude-frequency analysis, *J. Geol.*, *102*(1), 79–96.

Nitsche, F. O., W. B. F. Ryan, S. M. Carbotte, R. E. Bell, A. Slagle, C. Bertinado, R. Flood, T. Kenna, and C. McHugh (2007), Regional patterns and local variations of sediment distribution in the Hudson River Estuary, *Estuar. Coast. Shelf Sci.*, *71*(1–2), 259–277, doi:10.1016/j.ecss.2006.07.021.

Nitsche, F. O., T. C. Kenna, and M. Haberman (2010), Quantifying 20th century deposition in complex estuarine environment: An example from the Hudson River, *Estuar. Coast. Shelf Sci.*, *89*(2), 163–174, doi:10.1016/j.ecss.2010.06.011.

Nittrouer, C. A., S. A. Kuehl, R. W. Sternberg, A. G. Figueiredo Jr., and L. E. C. Faria (1995), An introduction to the geological significance of sediment transport and accumulation on the Amazon continental shelf, *Mar. Geol.*, *125*(3–4), 177–192, doi:10.1016/0025-3227(95)00075-A.

Nowacki, D. J., A. S. Ogston, C. A. Nittrouer, A. T. Fricke, and P. D. T. Van (2015), Sediment dynamics in the lower Mekong River: Transition from tidal river to estuary, *J. Geophys. Res. Oceans*, *120*(9), 6363–6383, doi:10.1002/2015JC010754.

Orton, P. M., and G. C. Kineke (2001), Comparing Calculated and Observed Vertical Suspended-Sediment Distributions from a Hudson River Estuary Turbidity Maximum, *Estuar. Coast. Shelf Sci.*, *52*(3), 401–410, doi:10.1006/ecss.2000.0747.

Panuzio, F. L. (1965), Lower Hudson River siltation., in *Proceedings of the 2nd Federal Interagency Sedimentation Conference*, pp. 512–550, Agricultural Research Service, Jackson, MS.

Ralston, D. K., and W. R. Geyer (2009), Episodic and Long-Term Sediment Transport Capacity in The Hudson River Estuary, *Estuaries Coasts*, *32*, 1130–1151, doi:10.1007/s12237-009-9206-4.

Ralston, D. K., W. R. Geyer, and J. A. Lerczak (2008), Subtidal Salinity and Velocity in the Hudson River Estuary: Observations and Modeling, *J. Phys. Oceanogr.*, *38*(4), 753–770.

Ralston, D. K., W. R. Geyer, and J. C. Warner (2012), Bathymetric controls on sediment transport in the Hudson River estuary: Lateral asymmetry and frontal trapping, *J. Geophys. Res.*, *117*(C10), C10013, doi:10.1029/2012JC008124.

Ralston, D. K., J. C. Warner, W. R. Geyer, and G. R. Wall (2013), Sediment transport due to extreme events: The Hudson River estuary after tropical storms Irene and Lee, *Geophys. Res. Lett.*, *40*(20), 2013GL057906, doi:10.1002/2013GL057906.

Rodenburg, L. A., and D. K. Ralston (2017), Historical sources of polychlorinated biphenyls to the sediment of the New York/New Jersey Harbor, *Chemosphere*, *169*, 450–459, doi:10.1016/j.chemosphere.2016.11.096.

Sanford, L., S. Suttles, and J. Halka (2001), Reconsidering the physics of the Chesapeake Bay estuarine turbidity maximum, *Estuaries Coasts*, *24*(5), 655–669, doi:10.1007/BF02804824.

Schubel, J. R., and D. J. Hirschberg (1978), Estuarine graveyards, climatic change, and the importance of the estuarine environment, in *Estuarine Interactions*, pp. 285–303, Academic Press, New York.

Shchepetkin, A. F., and J. C. McWilliams (2005), The regional oceanic modeling system (ROMS): a split-explicit, free-surface, topography-following-coordinate oceanic model, *Ocean Model.*, *9*(4), 347–404, doi:10.1016/j.ocemod.2004.08.002.

Sommerfield, C. K. (2006), On sediment accumulation rates and stratigraphic completeness: Lessons from Holocene ocean margins, *Cont. Shelf Res.*, *26*(17–18), 2225–2240, doi:10.1016/j.csr.2006.07.015.

Sommerfield, C. K., and K.-C. Wong (2011), Mechanisms of sediment flux and turbidity maintenance in the Delaware Estuary, *J. Geophys. Res.*, *116*, 16 PP., doi:201110.1029/2010JC006462.

Swaney, D. P., D. Sherman, and R. W. Howarth (1996), Modeling Water, Sediment and Organic Carbon Discharges in the Hudson-Mohawk Basin: Coupling to Terrestrial Sources, *Estuaries*, *19*(4), 833–847, doi:10.2307/1352301.

Syvitski, J. P. M. (2003), Supply and flux of sediment along hydrological pathways: research for the 21st century, *Glob. Planet. Change*, *39*(1–2), 1–11, doi:10.1016/S0921-8181(03)00008-0.

Traykovski, P., R. Geyer, and C. Sommerfield (2004), Rapid sediment deposition and fine-scale strata formation in the Hudson estuary, *J. Geophys. Res.*, *109*, F02004, doi:10.1029/2003JF000096.

Wall, G., E. Nystrom, and S. Litten (2008), Suspended Sediment Transport in the Freshwater Reach of the Hudson River Estuary in Eastern New York, *Estuaries Coasts*, doi:10.1007/s12237-008-9050-y.

Warner, J. C., W. R. Geyer, and J. A. Lerczak (2005), Numerical modeling of an estuary: A comprehensive skill assessment, *J. Geophys. Res.*, *110*, C05001, doi:10.1029/2004JC002691.

Warner, J. C., C. R. Sherwood, R. P. Signell, C. K. Harris, and H. G. Arango (2008), Development of a three-dimensional, regional, coupled wave, current, and sediment-transport model, *Comput. Geosci.*, *34*(10), 1284–1306, doi:10.1016/j.cageo.2008.02.012.

Warner, J. C., W. Rockwell Geyer, and H. G. Arango (2010), Using a composite grid approach in a complex coastal domain to estimate estuarine residence time, *Comput. Geosci.*, *36*(7), 921–935, doi:10.1016/j.cageo.2009.11.008.

Woodruff, J. D. (1999), Sediment deposition in the lower Hudson River estuary, M.S. thesis, Massachussets Institute of Technology/Woods Hole Oceanographic Institution.

Woodruff, J. D., W. R. Geyer, C. K. Sommerfield, and N. W. Driscoll (2001), Seasonal variation of sediment deposition in the Hudson River estuary, *Mar. Geol.*, *179*(1–2), 105–119, doi:10.1016/S0025-3227(01)00182-7.

Woodruff, J. D., A. P. Martini, E. Z. Elzidani, T. J. Naughton, D. J. Kekacs, and D. G. MacDonald (2013), Off-river waterbodies on tidal rivers: Human impact on rates of infilling and the accumulation of pollutants, *Geomorphology*, *184*, 38–50.

Zhang, W. G., J. L. Wilkin, and O. M. E. Schofield (2009), Simulation of Water Age and Residence Time in New York Bight, *J. Phys. Oceanogr.*, *40*(5), 965–982, doi:10.1175/2009JPO4249.1.

APPENDIX 1: Research products

Funding from this grant supported work on and is acknowledged in two manuscripts, one recently published and one that will be submitted shortly.

Rodenburg, L. A., and D. K. Ralston, 2017. "Historical sources of polychlorinated biphenyls to the sediment of the New York/New Jersey Harbor." *Chemosphere* 169: 450-459.

Ralston, D. K. and W. R. Geyer. “Sediment age in a tidal river”, in prep for *J. Geophys. Res.*

Results from this research were also presented at several seminars.

Ralston, D. K., “The role of the Mohawk River in Hudson River sediment dynamics”, Hudson River Environmental Society, New Paltz, NY, May 2016.

Ralston, D. K., “Long and muddy or short and sandy? How similar estuarine processes and forcing can lead to very different sedimentary environments”, University of Washington, Dept of Civil and Environmental Engineering, Mar 2016.

Ralston, D. K., “Linking Sediment Transport in the Hudson from the Tidal River to the Estuary”, Hudson River Foundation seminar, Oct 2015.

APPENDIX 2: Additional results from observations in 2014 and 2015

This appendix includes additional details on the observations collected in the tidal Hudson in 2014 and 2015. The observation periods did not capture any extreme discharge events as hoped, but they do provide important context for the effects of the seasonal and interannual variation in discharge on sediment transport in in the tidal river. In 2014, a typical spring freshet included several discharge events in the range of 2000-3000 $m^3 s^{-1}$ (Fig. A1). In 2015, discharge was lower than average through most of the winter and spring.

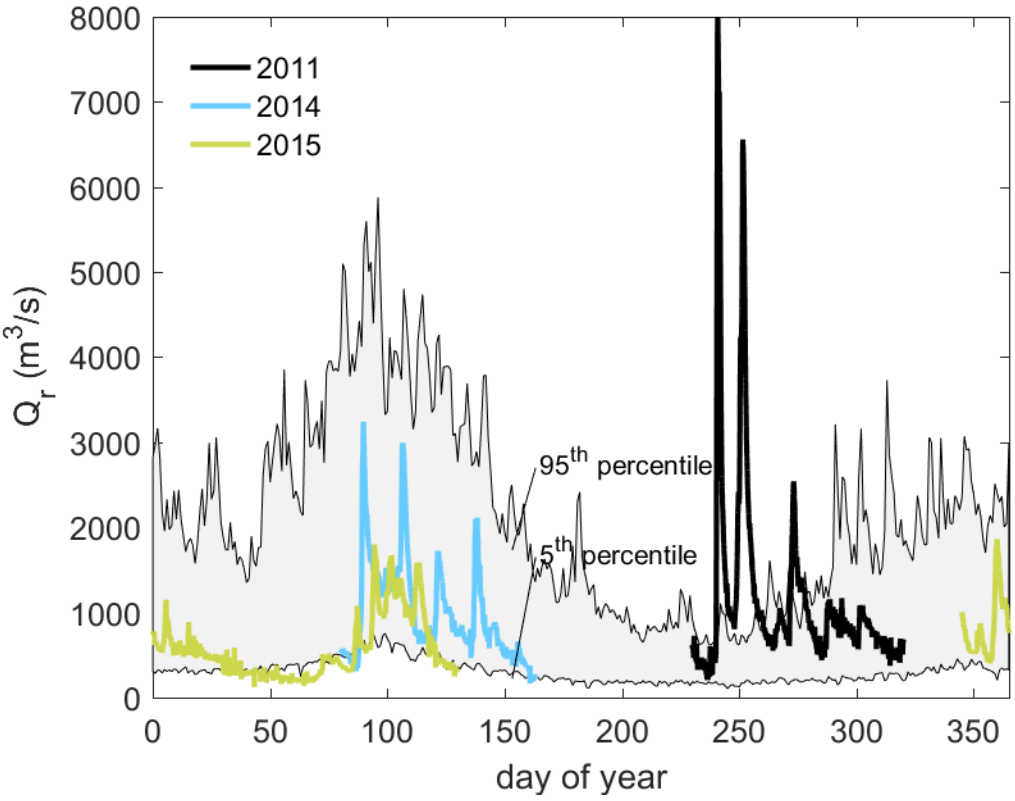

Figure A1. Discharge compared with climatology. Discharge includes all of the gauged tributaries of the Lower Hudson during observation periods and is plotted by day of year for summer 2011 (Irene and Lee), spring 2014, and winter/spring 2015. Thin lines represent the 5th and 95th percentiles for the combined Mohawk and Upper Hudson multiplied by a factor of 1.4 to account for inputs from Lower Hudson tributaries.

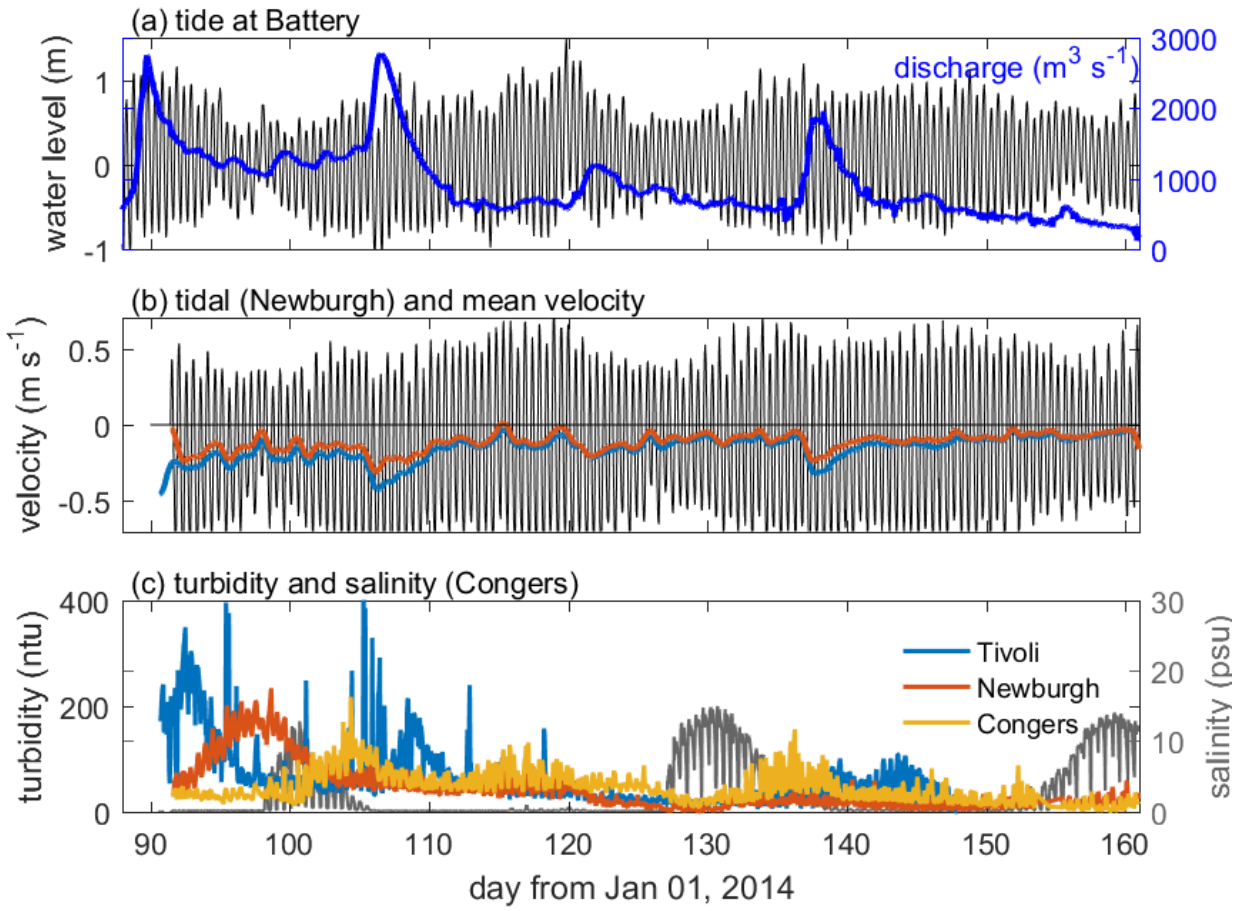

Figure A2. Time series at the mooring locations in spring 2014. (a) Water level at the Battery and river discharge. (b) Depth-averaged velocity at Newburgh (black) and tidally filtered velocity at Newburgh and Tivoli. (c) Near-bottom turbidity at Congers, Newburgh, and Tivoli; also plotted is near-bottom salinity at Congers.

Observations from spring 2014

Background on the mooring locations and instrumentation can be found in the methods section of the report. For additional detail, here we plot the velocity and turbidity time series (Fig. A2). 2014 had several moderate discharge events, and the instruments were deployed at the start of the first event and captured the propagation of the turbidity signal along the tidal river. The second significant event had a similar maximum discharge, but the turbidity signal at each of the mooring locations was about half as large as in the first event. This is consistent with observations from other systems where the first discharge event after the spring thaw remobilizes

sediment that has slowly accumulated in the river during the lower discharge winter months, and the sediment available for resuspension is less during subsequent discharge events.

The depth-averaged tidal velocities at Newburgh varied with spring-neap forcing from 0.3 to 0.8 m s^{-1} (Fig. A2), and tidal velocities at Tivoli were similar in magnitude. The tidally filtered velocities varied with the river discharge, increasing to 0.4 m s^{-1} at Tivoli and 0.3 m s^{-1} at Newburgh during the larger discharge events. By the end of the observation period in June the discharge was about 300 m^3 s^{-1} and the mean velocities were about 0.05 m s^{-1} at both locations.

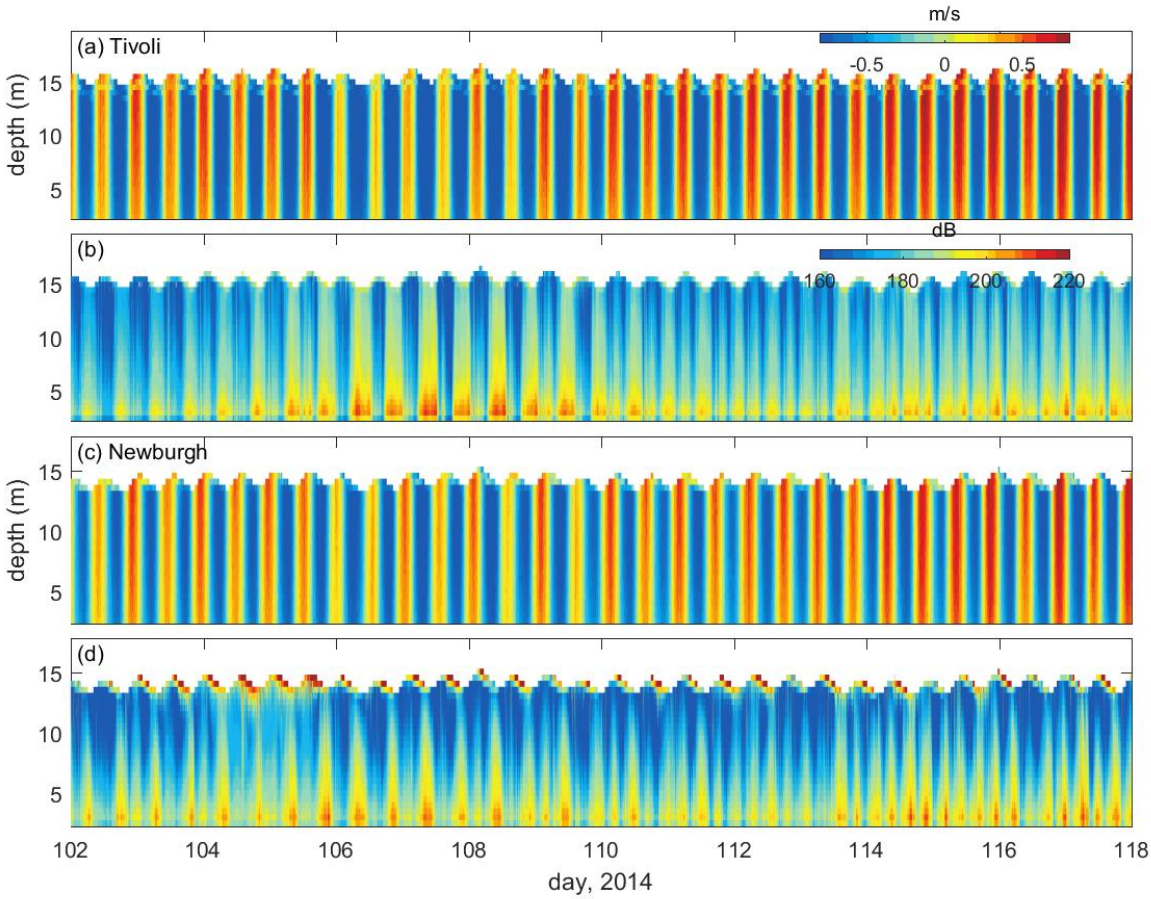

Figure A3. Time series of velocity and acoustic backscatter profiles during part of the observation period in 2014. (a) Velocity and (b) acoustic backscatter at Tivoli. (c) Velocity and (d) acoustic backscatter at Newburgh.

The correspondence between turbidity and discharge was clearest at Tivoli and decreased with distance downstream. Tidal resuspension was similar among the three locations, with tidal variation of 50-100 ntu early in the record and generally decreasing in amplitude during the

observation period. At Congers, tidal resuspension was most pronounced, particularly during spring tides after the salinity intrusion had reached that location during previous neaps. Increased tidal resuspension at those times is consistent with trapping of sediment in the frontal region near Croton Point during neap tides followed by remobilization and seaward advection during spring tides [*Ralston et al.*, 2013].

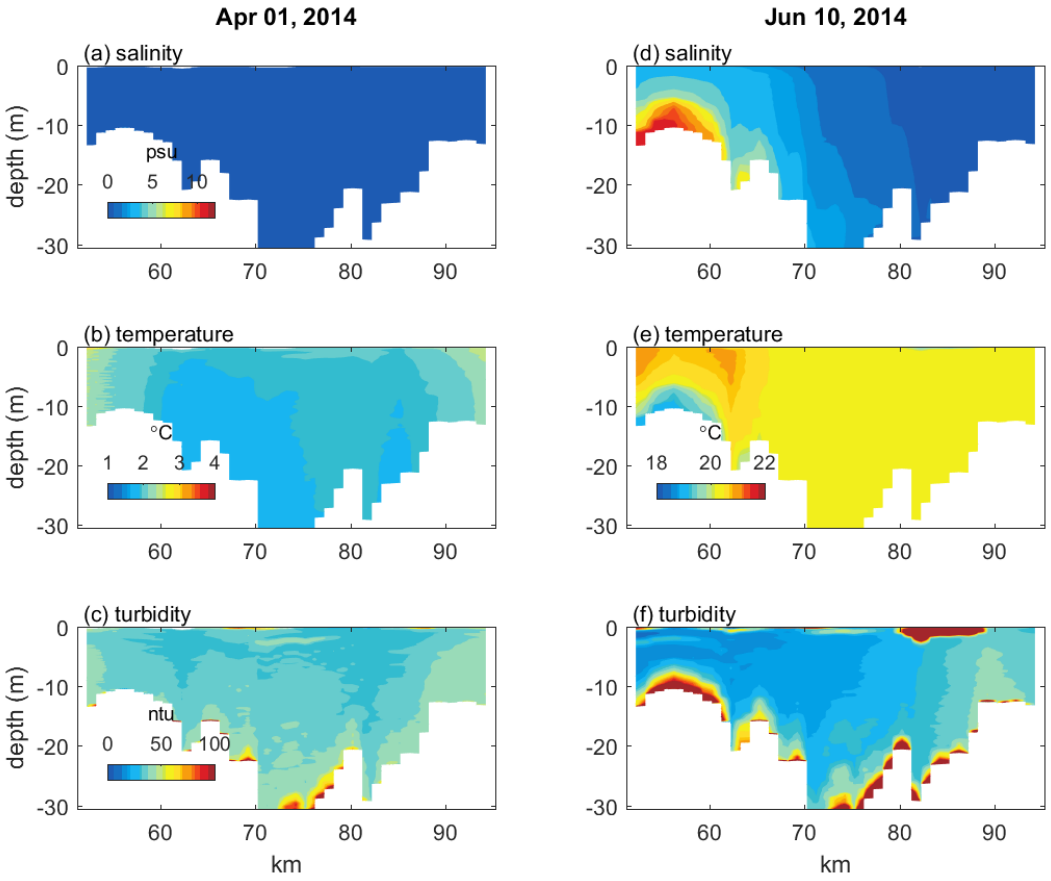

Figure A4. Along-river CTD and turbidity sections in spring 2014 between the Congers (55 km) and Newburgh (90 km) moorings. (a) Salinity, (b), temperature, and (c) turbidity during high discharge conditions at deployment (April 1, 2014). (d) Salinity, (e), temperature, and (f) turbidity during low discharge conditions at recovery (June 10, 2014). Note that the variables use the same color scale for both dates except temperature. High turbidity regions near the surface are artifacts from prop wash bubbles.

Acoustic backscatter can be used as a proxy for suspended sediment concentration, and the time series of backscatter and velocity profiles from the ADCPs highlight the combined tidal and fluvial processes driving sediment transport (Fig. A3). During the first part of the period shown,

the discharge event around day 106 dampened the flood tide velocities and enhanced ebb velocities, most notably at Tivoli. During this period, backscatter increased to its highest levels, but only during ebb tides, and during flood tides the backscatter dropped to near background levels. Because acoustic backscatter is proportional to particle volume (rather than cross-sectional area as for optical backscatter), the acoustic signal is more sensitive to large particles than to small particles, and consequently it may be underrepresenting the washload during this period. The signal did clearly show tidally modulated resuspension and settling, and with the much lower concentrations during flood tides is consistent with net seaward flux. Around 10 days later, the river discharge had decreased from 2500 $m^3 s^{-1}$ to about 500 $m^3 s^{-1}$, but spring tides had begun to increase velocities again. Acoustics backscatter increased during this period as well, but a key difference was that it was enhanced during both maximum flood and maximum ebb velocities, suggesting more symmetric tidal sediment flux and less seaward transport.

Along-river transects at deployment and recovery provide larger scale context of the seasonal changes across the study period (Fig. A4). At the start of the freshet, the survey region from Newburgh to Congers was entirely fresh, and there was little structure to the temperature distribution. Turbidity was elevated all along the river, with a background level of about 40 ntu that was independent of regions of local resuspension. In contrast, in the lower discharge conditions of June the salinity intrusion extended north of Haverstraw Bay and into the Hudson Highlands. Turbidity in the upper water column was less than in the spring, but regions of greater sediment concentration were found near the bed in several regions. In particular, increased concentrations in upper Haverstraw Bay were consistent with sediment trapping by the salinity intrusion during lower discharge periods.

Observations from winter/spring 2015

In the winter and spring of 2015 the discharge was lower than average and there were no discharge events over 2000 $m^3 s^{-1}$ (Fig. A5). The range of tidal velocities was similar to 2014, but the mean velocities were almost always less than 0.1 m s^{-1}. At times, particularly at the most seaward station at Congers, the mean velocity was landward due to low-frequency water level fluctuations (storm surge) in the coastal ocean driving changes in the volume of the estuary. The first discharge event of the seasons did have a proportionally larger turbidity signal than subsequent events, although instrument fouling hampered data quality toward the end of the

deployment. The dominant variation in the turbidity signal was spring-neap, particularly at Congers where the salinity intrusion was present almost every neap tide.

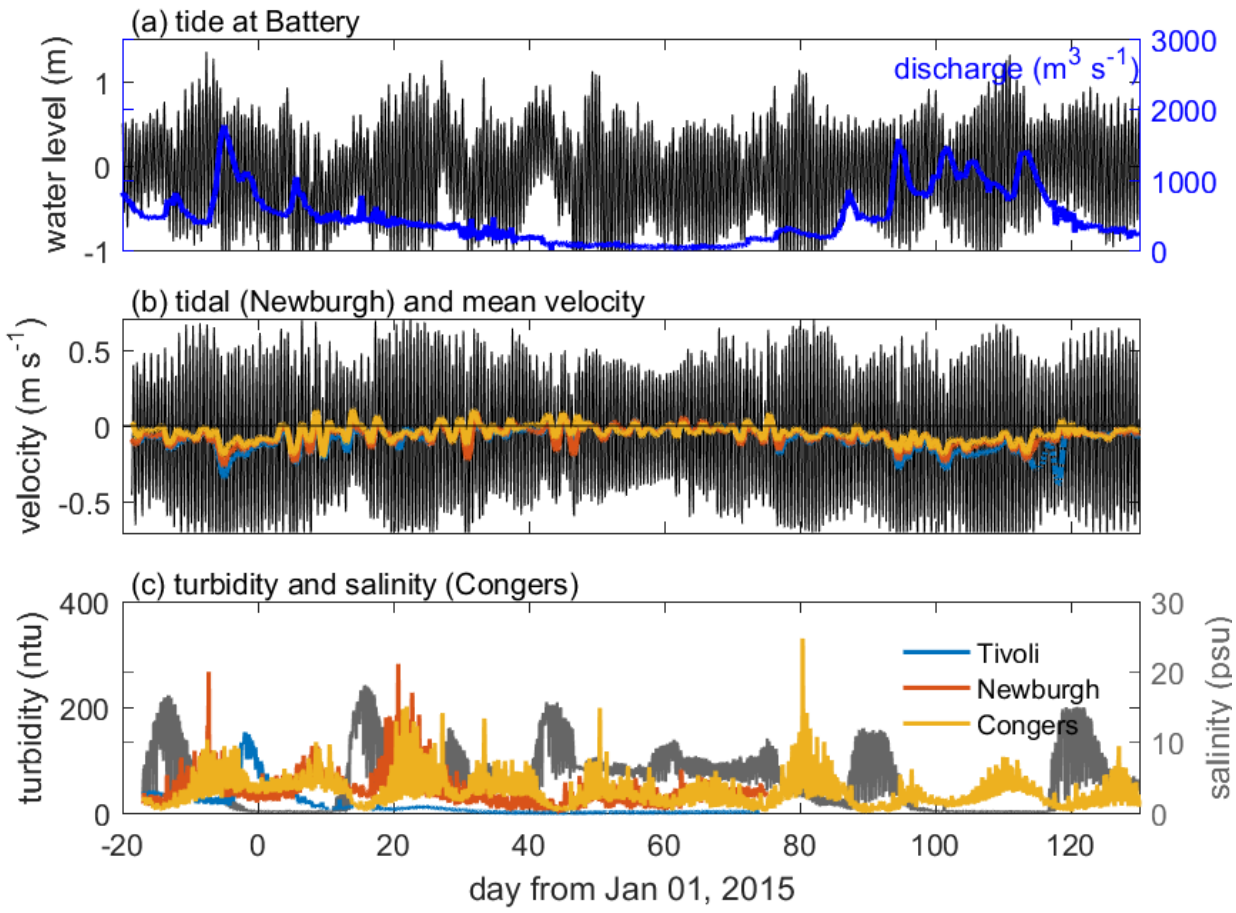

Figure A5. Time series at the mooring locations in winter and spring 2015. (a) Water level at the Battery and river discharge. (b) Depth-averaged tidal velocity at Newburgh (black) and tidally filtered velocity at Newburgh, Tivoli, and Congers. (c) Near-bottom turbidity at Congers, Newburgh, and Tivoli.

Along-river surveys reflect the lower discharge conditions throughout the study period, with salinity in the lower part of the survey region at both deployment and recovery (Fig. A6). Turbidity was concentrated near the bed particularly in a few zones of resuspension, unlike the high discharge of the first survey in 2014 when it was distributed more uniformly in the vertical and along-river. The long distances covered by the surveys (40-100 km) prohibit synoptic

sampling and lead to tidal aliasing that prevents detailed interpretation of the along-river structure.

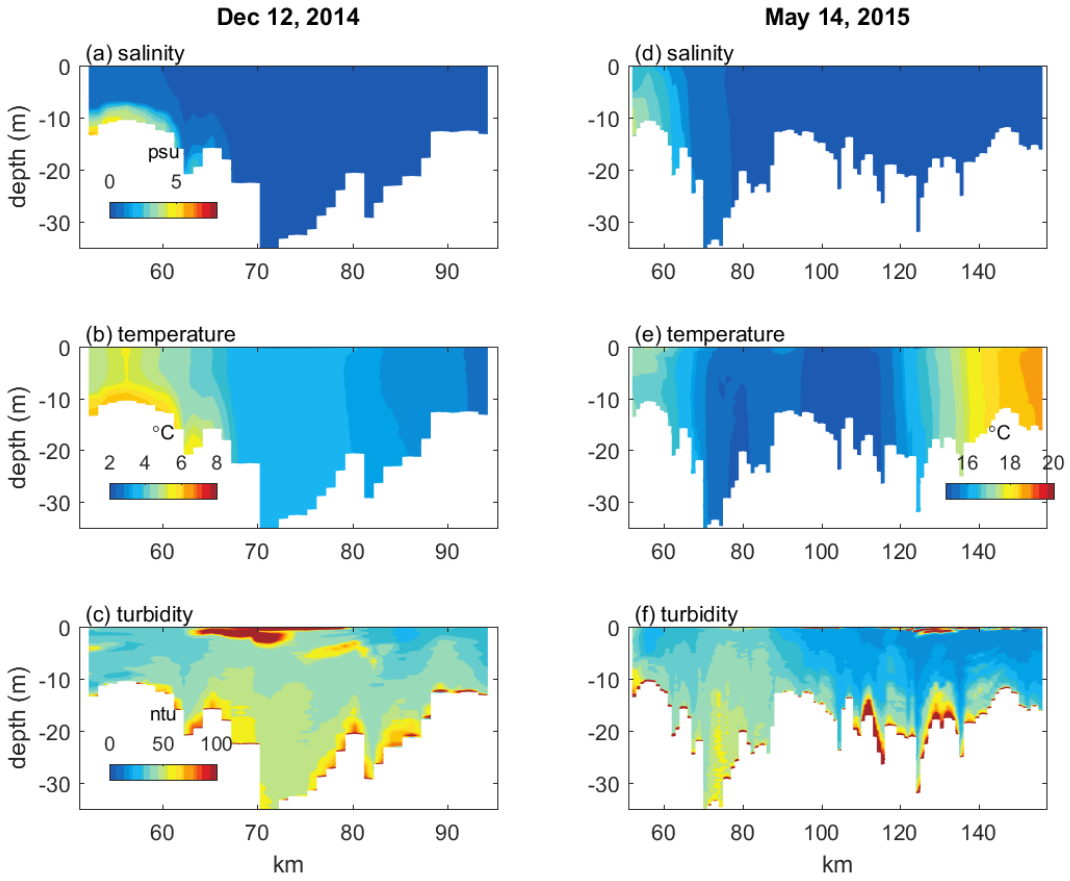

Figure A6. Along-river CTD and turbidity sections in December 2014 between the Congers (55 km) and Newburgh (90 km) moorings with (a) salinity, (b), temperature, and (c) turbidity. Along-river CTD and turbidity sections in May 2015 between the Congers (55 km) and Tivoli (160 km) moorings with (d) salinity, (e), temperature, and (f) turbidity. Note that the variables use the same color scale for both dates except temperature. High turbidity regions near the surface are artifacts from prop wash bubbles.